Differential geometry based solvation model II: Lagrangian formulation

Zhan Chen[1], Nathan A. Baker[2] and G. W. Wei[1,3*]
[1]Department of Mathematics
Michigan State University, MI 48824, USA
[2] Department of Biochemistry and Molecular Biophysics, Center for Computational Biology
Washington University in St. Louis
700 South Euclid Avenue, Campus Box 8036, St. Louis, Missouri 63110, USA
[3]Department of Electrical and Computer Engineering
Michigan State University, MI 48824, USA

May 28, 2010

Abstract

Solvation is an elementary process in nature and is of paramount importance to more sophisticated chemical, biological and biomolecular processes. The understanding of solvation is an essential prerequisite for the quantitative description and analysis of biomolecular systems. This work presents a Lagrangian formulation of our differential geometry based solvation model. The Lagrangian representation of biomolecular surfaces has a few utilities/advantages. First, it provides an essential basis for biomolecular visualization, surface electrostatic potential map and visual perception of biomolecules. Additionally, it is consistent with the conventional setting of implicit solvent theories and thus, many existing theoretical algorithms and computational software packages can be directly employed. Finally, the Lagrangian representation does not need to resort to artificially enlarged van der Waals radii as often required by the Eulerian representation in solvation analysis. The main goal of the present work is to analyze the connection, similarity and difference between the Eulerian and Lagrangian formalisms of the solvation model. Such analysis is important to the understanding of the differential geometry based solvation model. The present model extends the scaled particle theory (SPT) of nonpolar solvation model with a solvent-solute interaction potential. The nonpolar solvation model is completed with a Poisson-Boltzmann (PB) theory based polar solvation model. The differential geometry theory of surfaces is employed to provide a natural description of solvent-solute interfaces. The minimization of the total free energy functional, which encompasses the polar and nonpolar contributions, leads to coupled potential driven geometric flow and Poisson-Boltzmann equations. Due to the development of singularities and nonsmooth manifolds in the Lagrangian representation, the resulting potential-driven geometric flow equation is embedded into the Eulerian representation for the purpose of computation, thanks to the equivalence of the Laplace-Beltrami operator in the two representations. The coupled partial differential equations (PDEs) are solved with an iterative procedure to reach a steady state, which delivers desired solvent-solute interface and electrostatic potential for problems of interest. These quantities are utilized to evaluate the solvation free energies and protein-protein binding affinities. A number of computational methods and algorithms are described for the interconversion of Lagrangian and Eulerian representations, and for the solution of the coupled PDE system. The proposed approaches have been extensively validated. We also verify that the mean curvature flow indeed gives rise to the minimal molecular surface (MMS) and the proposed variational procedure indeed offers minimal total free energy. Solvation analysis and applications are considered for a set of 17 small compounds and a set of 23 proteins. The salt effect on protein-protein binding affinity is investigated with two protein complexes

---

*Please address correspondence to Guowei Wei. E-mail:wei@math.msu.edu

by using the present model. Numerical results are compared to the experimental measurements and to those obtained by using other theoretical methods in the literature.

Key words: Differential geometry based multiscale model, Poisson-Boltzmann equation, Potential driving geometric flows, Solvation free energy, Implicit solvent model, Laplace-Beltrami operator, Protein-protein interaction.

Contents

I Introduction

Almost all important biological processes in nature, including signal transduction, DNA recognition, transcription, post-translational modification, translation, protein folding and protein ligand binding, occur in water, which comprises 65-90% of cellular mass. The understanding of solvation is an elementary prerequisite for the quantitative description and analysis of the above-mentioned processes. Solvation involves the energetics of interactions between solute molecules and solvent molecules or ions in the aqueous environment. Solute-solvent interactions are typically described by solvation energies (or closely related quantities): the free energy of transferring the solute from a vacuum to the solvent environment of interest (e.g., water at a certain ionic strength), as shown in more detail in Fig. 1. Solvation free energy is a physical quantity that can be measured by experiments. To help the calculation of solvation energy, one can conceptually break up
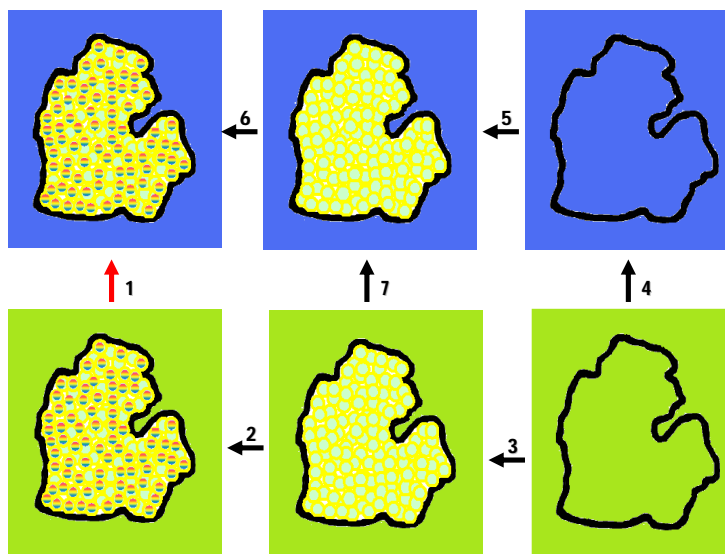

Figure 1: A solvation free energy cycle adapted from Levy et al.[118] The total solvation energy (1) is decomposed into several steps: "charging" the solute in solvent (6) and vacuum (2), including attractive dispersive solute-solvent interactions in solvent (5) and vacuum (3), and cavity formation associated with repulsive solute-solvent interactions (4). The energy associated with Step (7) is generally termed a "nonpolar solvation energy" while the difference in energies associated with Steps (1) and (7) is generally considered as "polar solvation energy".

the solvation process as the follows: #1 in this figure can be decomposed into two basic processes: a "nonpolar" process of inserting the uncharged solute into solvent (#7) and a "polar" process of charging the solute in vacuum (#2) and solvent (#6). The free energy change in #7 is called the nonpolar solvation energy. The difference of energies associated with #6 and #2 is called the "charging" or polar solvation energy and represents the solvent's effect on the solute charging process. The polar portion of solvation originates from electrostatic interactions, which are ubiquitous for any system of charged or polar molecules, such as biomolecules (proteins, nucleic acids, lipid bilayers, sugars, etc.) in their aqueous environment.[6,8,57,61,72,75,92,184–186,216,217] The nonpolar portion describes the remaining contributions, including the surface tension, mechanical work, and attractive solvent-solute dispersion interactions.

Solvation free energies can be calculated by a variety of computational methods ranging from very time-consuming quantum mechanical approaches[99,107,136,169] to simple phenomenological modifications of Coulomb's law. Solvation models can be roughly divided into two main classes:[171,184,185,216] explicit solvent models that describe the solvent in molecular or atomic,[165] and implicit solvent models that generally replace the explicit solvent with a dielectric continuum.[7,9,57,96,106,171] Explicit solvent models provide the detailed information on molecular constitutions, and generally require extensive sampling to extract meaningful thermodynamic, statistical or kinetic properties of interest. Whereas implicit solvent models focus on the biomolecules of interest, and take a mean field approximation for solvent properties. Because of their fewer degrees of freedom, implicit solvent methods have become popular for many applications in molecular simulation.[6,8,61,72]

Electrostatic interactions are ubiquitous in nature. For biomolecular systems in aqueous environment, the analysis of molecular solvation and electrostatics is of great importance to research in chemistry, biophysics, medicine and nano-technology. Implicit solvent models are widely used in such an analysis which can be classified into two general types: quantitative analysis and qualitative study. One of the primary quantitative application in computational biology and chemistry has been the calcula-

4

tion of thermodynamic properties. Implicit solvent methods "pre-equilibrate" the solvent and mobile ions, thus effectively pre-compute the solvent contribution for a system.[171] Such pre-equilibration is particularly evident in MM/PBSA models,[137,160,196,201,224] which combine implicit solvent approaches with molecular mechanical models to evaluate binding free energies from an ensemble of biomolecular structures.[3,14,84,119–121,133,138,149,150,150,204,229] These methods have been employed to interpret experimental titration curves, analyze residue contributions in protein-protein and protein-ligand binding energetics, examine structural/functional consequences of RNA nucleotide protonation, etc. Another quantitative application of implicit solvent models is the evaluation of biomolecular kinetics where implicit solvent models are generally taken to compute solvation forces for molecular Langevin dynamics,[129,130,166,167,200] Brownian dynamics,[69,78,135,179] or continuum diffusion[44,45,191,192,233] simulations. A major qualitative study of implicit solvent methods is the visualization and qualitative analysis of electrostatic potentials on and around biomolecular surfaces.[6,10,163,218] Visualization has become a standard procedure in the analysis of biomolecular structures, including ligand-receptor binding, drug design, macromolecular assembly, protein-nucleic acid complexes, protein-protein interactions, enzymatic mechanism study, etc.

Polar solvation process and electrostatic effect are described by a variety of implicit solvent models;[8,9,37,57,81,109,171,178,182,184,202,212,216,217] however, the most widely-used ones are Poisson-Boltzmann (PB) models,[6,57,61,75,92,106,112,184] generalized Born (GB) methods[13,37,60,81,89,109,144,155,206,208,241] and polarizable continuum models (PCM).[12,30,47,53,101,198,207] Polarizable continuum models are proposed to model the solvent either as polarizable dielectrics or as conductor-like media, and treat the solute compound by the quantum mechanical means.[12,30,47,53,101,198,207] These approaches have often been used in reactively kinetics where quantum mechanical descriptions are desired. Generalized Born methods are relatively fast, but are not as accurate as the PB methods.[8,55,60,154,154,206,209] They are often employed in high-throughput applications such as molecular dynamics.[13,37,55,60,72,109,155,185,208] PB methods can be formally derived from more detailed theories[19,94,147] and provide a more accurate, although somewhat slower, approach for evaluating polar solvation properties.[13,55,154] Moreover, unlike most generalized Born methods, PB models offer a global description for the electrostatic properties, therefore making them uniquely suited to visualization and other study[25,56,58,69,78,126,180,192,213] where the electrostatic information is required for both inside and outside a biomolecule.

The separation of discrete and continuum domains in implicit solvent models requires an interface to indicate the separation of solute atoms from the surrounding solvent. Naturally, such an interface can be regarded as the surface or the profile of a molecule. The definition of molecular profiles, or molecular graphics traces back to Corey and Pauling in 1950s,[52] who tried to depict the profiles of amino acids, peptides and proteins from X-ray crystallography. In quantum chemistry, molecular graphics are often associated with the shapes of polynomial functions that provide approximation to electron wavefunctions. In fact, since the electron wavefunction changes its distribution under different environments, molecular profiles change accordingly. Commonly used interface definitions in implicit solvent models include the van der Waals surface, the solvent accessible surface,[114] and the molecular surface (MS).[51,170] In certain sense, these interface definitions determine the performance of implicit solvent models because all of the physical properties of interest, including electrostatic free energies, biomolecular surface areas, molecular cavitation volumes, solvation free energies, and pK_a values are very sensitive to these interface definitions.[62,64,151,197]

Current two-scale implicit solvation models have a severe limitation that undermines their performance in practical applications. While traditional surface definitions have found much success in biomolecular modeling and computation,[22,54,65,103,110,124,127,193] they are simply *ad hoc* divisions of the solute and solvent regions of the problem domain. In reality, the solvation is a physical process and its equilibrium state should be determined by fundamental laws of physics. Moreover, these surface definitions admit non-smooth interfaces, i.e., cusps and self-intersecting surfaces, that lead to well-known instability in molecular simulations due to extreme sensitivity to atomic positions, radii, etc.[173] This sensitivity often drives the use of alternative "smoothed" solvent-solute interface definitions[88,100] that can introduce additional computational artifacts.[62,64] Furthermore, the wide range of surface definitions has often led to

confusion and misuse of parameter (radii) sets developed for implicit solvent calculations with specific surface definitions.

The recent development of a new class of molecular interfaces that incorporate the fundamental laws of physics starts with the construction of partial differential equation (PDE) based molecular surface by Wei el al. in 2005.[223] This approach distinguishes itself from many other PDE based surface smoothing methods[227,234] by utilizing only atomic information, i.e., atomic coordinates and radii, instead of an existing surface. The atomic information is embedded in the Eulerian formulation and a family of hypersurfaces are evolved in time under the PDE operator, which is designed to control the curvature and surface tension. The generalized molecular surface is subsequently extracted from the final hypersurface by a level-set type of approach.[223] This PDE based surface construction procedure generates well defined molecular surfaces for both small molecules and large proteins.[223] To our knowledge, geometric PDE based approach was the first of its kind for molecular surface construction. A further progress in the development of a "physical interface" was the introduction of the minimal molecular surface (MMS) that minimizes a surface free energy functional by the variational principle and leads to the mean curvature flow in 2006.[16,17] To our knowledge, MMSs were the first set of biomolecular surfaces that had ever been constructed by means of variational principles. The construction of the MMS was driven by the desire to understand the true physical boundary of a biomolecule in solvent. As a physical concept, the solvent-solute interface should be in general determined by the minimization of the free energy of the macromolecule in the aquatic environment. The MMS is constructed by using essentially the same procedure as that developed in the first PDE based surface generation method.[223] Another desirable property of the MMS is that it is free of geometric singularities. The MMS model was applied to the calculation of electrostatic solvation free energies of 26 proteins.[18] However, the MMS, which incorporates only the minimization of the free energy associated with the surface tension, offers only an approximation to the true physical boundary of a biomolecule in solvent. Moreover, the representation of the surface by the Gram determinant and hypersurface is also an approximation. More rigorous definition was given by the geometric measure theory.[221] To account for other important effects that determining the solvent-solute interface, we have recently proposed potential driven geometric flows (PDGFs) that allow the incorporation of many other potential effects in surface formation and evolution.[15] The PDGFs are inherently multiscale in nature, and enable the incorporation of microscopic interactions, such as van der Waals potentials, into the macroscopic curvature evolution.

Another criticism of implicit solvent models is the lack of uniqueness in polar and nonpolar decomposition of the solvation process[136] and the neglect of the polar-nonpolar coupling as well as solvent-solute interactions.[4,28,34,49,66,74,76] Dzubiella et al[66,67] considered this problem by adding a solvent-solute coupling (interaction) term to the total free energy functional discussed by Sharp and Honig[184] and Gilson et al.[86] A feature of this new model is that surface tension energy and mechanical work of immersing a molecule into the solvent were also included in the total free energy functional. However, their initial work does not provide a protocol for the construction of molecular interfaces and systematical analysis of solvation energy for macromolecules. Recently, Cheng et al.[43] have extracted solvent-solute interfaces from the free energy functional of Dzubiella et al[66,67] in a setting very similar to our earlier Eulerian geometric PDE approaches of biomolecular surfaces and solvation analysis.[16–18,223]

Much of the recent development in implicit solvent models is due to the use of geometric flows,[15,16,18,221,223] particularly mean curvature flows, which have been of considerable interest in applied mathematics for decades.[73,87,140,156,158,172,175,177,181,181,190,225] Earlier research work and part of present research are focused on image processing,[158,172] computer vision, materials design[181] and surface smoothing.[227,234] Computational techniques using the level set theory were devised by Osher and Sethian[158,172,181] and have been further developed and applied by many others.[33,48,188] An alternative approach for image analysis is to minimize a functional in the framework of the Mumford-Shah variational functional,[146] and/or the Euler-Lagrange formulation of variation.[26,32,122,157,172,174] We introduced some of the first family of high-order geometric flow equations for image analysis.[220] In fact, the nonlinear production term in these high-order operators provides a framework to accommodate the PDGF in our later formation for macromolecular surfaces. Our high-order geometric flow equations have led to many interesting

applications.[35,85,132,195,220,222] Mathematical analysis of these high order equations in Sobolev space was carried out by Bertozzi and Greer,[24,90,91] who proved the existence and uniqueness of the solution to a case with H^1 initial data and a regularized operator. A similar analysis was performed by Xu and Zhou.[228] We also introduced a coupled geometric flow equation system for image edge detection.[222] Such an algorithm works extremely well with texture images. Recently, we have proposed an evolution operator based single-step method for image denoising and enhancement.[195] Most recently, a family of differential geometry based multiscale models have been developed for chemical and biomolecular systems, including fuel cells, ion channels, DNA packing, nanofluidic systems, and virus evolution.[221] These models describe not only the structure, but also the dynamics and transport of the above mentioned chemical and biomolecular systems.

Most recently, we have extended our earlier variational formulation of surface free energy[16–18] to the analysis of the total solvation free energy[42] via differential geometry theory of surfaces. Such an analysis makes use of the geometry measure theory to represent the surface area density of the solute molecule by the gradient of the hypersurface function, which can be regarded as the characteristic function of the solute molecule, and provides a smooth representation of the solvent-solute interface. With this area representation, we construct a total free energy functional of solvation. The variation of the total free energy functional leads to coupled generalized Poisson-Boltzmann equation and the generalized Laplace-Beltrami equation. The latter governs the formation and evolution of the solute characteristic function. This set of coupled nonlinear PDEs minimizes the total free energy functional. In this approach, the total free energy functional encompasses not only the curvature effect, the mechanical work and the electrostatic energy, but also the solvent-solute interactions. Although the spirit of the present approach is similar to that of Sharp and Honig,[183] Gilson et al.,[86] Dzubiella et al.,[66,67] and our earlier work,[16,18] the present work is unique in its rigorous implementation of differential geometry theory of surfaces. The numerical realization of the new solvation model was carried by using the protocol of the PDE based molecular surface construction established in the past few years.[15–18,223]

In terms of computation, the formation and evolution of biomolecular surfaces can be described by either the Lagrangian formulation or the Eulerian formulation. In the Lagrangian formalism, surface elements are directly evolved according to a governing equation or a set of rules. In the Eulerian formalism, the surface is embedded in a hypersurface function, or a level set function, and such a function is evolved under prescribed physical and/or biological principles.[18,42] A sharp surface can be obtained from an isosurface extraction procedure, such as the level set approach. Usually, the Lagrangian formalism is straightforward for force prescription as shown in our earlier work[15] and is computationally efficient, but typically encounters difficulties in handling geometric singularities, such as surface break-up or surface merging. In terms of solvation analysis, the Lagrangian representation of biomolecular surfaces offers a basis for visualization, surface electrostatic potential map and visual perception of biomolecules. Additionally, the Lagrangian representation is consistent with the conventional setting of the Poisson-Boltzmann theory. As such, many existing theoretical algorithms and software packages can be applied directly. Finally, the Lagrangian representation avoids the use of artificially enlarged van der Waals radii as often required by smooth surface models.[42,214]

In principle, an isolated molecule can be analyzed by the first principle — a quantum mechanical description of the wavefunction or density distribution of all the electrons and nuclei. However, such a description is computationally intractable for large biomolecules. Under physiological condition, biomolecules are in a non-isolate environment, and are interacting with solvent molecules and/or other biomolecules. Therefore, their wavefunctions overlap spatially, so do their electron density distributions. Consequently, there is no sharp interface between the solvent and the solute. The Eulerian formulation is important in the sense that is able to produce an overlapping solvent-solute boundary, which may be able to describe the true physical boundary between the solvent and solute when its generation is governed by the variational principle — the total free energy minimization.[42,221] Moreover, Eulerian formulation is important because it is able to handle topological changes during the surface evolution. Finally, Eulerian formalism provides a convenient approach for multiscale analysis.[221] In summary, Lagrangian and Eulerian formulations of solvation models are complementary to each other in many aspects and are both

important and valuable.

The objective of the present work is to explore the Lagrangian formulation of the differential geometry based solvation model, and analyze the similarity and difference of two differential geometry based formulations. The mathematical analysis of biomolecular surfaces in the Lagrangian formulation is quite different from that of the Eulerian formulation. The Lagrangian analysis of biomolecular surfaces makes the direct use of differential geometry theory of surfaces and manifolds. The surface minimization leads to the Laplace-Beltrami operator, or the mean curvature operator. Whereas the Eulerian analysis of biomolecular surfaces utilizes the coarea theorem of the geometric measure theory. The resulting operator from surface area minimization can also be identified as a generalized Laplace Beltrami operator in a higher dimension. The connection of two representations is analyzed in the present work. The structure of governing equations, and the accuracy and efficiency of two formulations are compared.

The rest of this paper is organized as follows. In Section II, we present the Lagrangian formulation of differential geometry based solvation models. The total free energy functional of solvation is constructed, and followed by detailed analysis of on-manifold variations. Such variations produce coupled potential driven geometric flow and Poisson-Boltzmann equations. Section III is devoted to the computational methods and algorithms. We discuss different realizations of biomolecular surfaces, including direct on-manifold evolution and Eulerian embedding approaches. Algorithms for Eulerian and Lagrangian inter converting are also discussed. A solution strategy for the coupled equations is designed and analyzed. The proposed PDE methods are of second order in convergence. Method for solvation free energy calculations is also given. The proposed methods and algorithms are validated in Section IV. A large number of numerical examples are designed to test the numerical accuracy, convergence order and computational efficiency of computational methods and algorithms. The proposed differential geometry based solvation model is applied to two classes of problems in Section V. First, we examine the solvation free energy calculation of a set of small molecules. We then extend our solvation calculations to a set proteins. Results are compared with experimental data, those obtained by using our earlier Eulerian formulation and those obtained by the classic molecular surface definition. Finally, we consider two cases of salt-regulated protein-protein interactions. The protein binding affinities are computed by using the proposed new models. The resulting binding affinities compare well with experimental data in the literature. This paper ends with a conclusion.

II Theory and model

This section presents the differential geometry based solvation model. We first review the theory of surfaces and curvatures for smooth manifolds. We then discuss a few free energy functionals of solvation. These functionals may appear exactly the same as the solvation energy expressions in the classic theory of solvation. However, a fundamental difference is that, in the present approach, the solvent-solute interface will be obtained by the variational principle, rather than by a prefixed surface, such as the van der Waals surface or the molecular surface. The governing equations for the solvation system, including the Poisson-Boltzmann equation and the generalized Laplace Beltrami equation, will be derived from the first variation.

II.A Manifold and curvature preliminary

In this work, we consider the solvent-solute boundary as a 2-dimensional (2D) differentiable manifold embedded in a 3D Euclidean space or a hypersurface in a Riemannian manifold. Therefore, the subsequent free energy minimization can be carried out on the 2D manifold. For example, the area of a solvent-solute interface is modeled as a surface integration over the biomolecular manifold. Therefore, it is necessary to present a brief review of manifolds and curvatures[15,18] so as to establish notations and provide basic ideas for the further theoretical development.

Consider a C^2 immersion $\mathbf{f} : U \to \mathbb{R}^{n+1}$, where $U \subset \mathbb{R}^n$ is an open set and $\overline{U}$ is compact.[226] Here $\mathbf{f}(\mathbf{u}) = (f_1(\mathbf{u}), f_2(\mathbf{u}), \cdots, f_{n+1}(\mathbf{u}))$ is a hypersurface element (or a position vector), and $\mathbf{u} = (u_1, u_2, \cdots, u_n) \in U$. Tangent vectors (or directional vectors) of $\mathbf{f}$ are $X_i = \frac{\partial \mathbf{f}}{\partial u_i}, i = 1, 2 \cdots n$. The Jacobi matrix of the mapping $\mathbf{f}$ is given by $D\mathbf{f} = (X_1, X_2, \cdots, X_n)$. The first fundamental form is a symmetric, positive definite metric tensor of $\mathbf{f}$, given by $I(X_i, X_j) := (g_{ij}) = (D\mathbf{f})^T \cdot (D\mathbf{f})$. Its matrix elements can also be expressed as $g_{ij} = \langle X_i, X_j \rangle$, where $\langle , \rangle$ is the Euclidean inner product in $\mathbb{R}^n$,

$i, j = 1, 2, \cdots, n$.

Let $\mathbf{N}(\mathbf{u})$ be the unit normal vector given by the Gauss map $\mathbf{N} : U \to R^{n+1}$,

$$\mathbf{N}(u_1, u_2, \cdots, u_n) := X_1 \times X_2 \cdots \times X_n / \|X_1 \times X_2 \cdots \times X_n\| \in \perp_{\mathbf{u}} \mathbf{f}, \tag{1}$$

where "$\times$" denotes the cross product. Here $\perp_{\mathbf{u}} \mathbf{f}$ is the normal space of $\mathbf{f}$ at point $\mathbf{X} = \mathbf{f}(\mathbf{u})$, where the position vector $\mathbf{X}$ differs much from tangent vectors X_i. The normal vector $\mathbf{N}$ is perpendicular to the tangent hyperplane $T_{\mathbf{u}} \mathbf{f}$ at $\mathbf{X}$. Note that $T_{\mathbf{u}} \mathbf{f} \oplus \perp_{\mathbf{u}} \mathbf{f} = T_{\mathbf{f}(\mathbf{u})} \mathbb{R}^n$, the tangent space at $\mathbf{X}$. By means of the normal vector $\mathbf{N}$ and tangent vector X_i, the second fundamental form is given by

$$II(X_i, X_j) = (h_{ij})_{i,j=1,2,\cdots n} = \left(\left\langle -\frac{\partial \mathbf{N}}{\partial u_i}, X_j \right\rangle \right)_{ij}. \tag{2}$$

The mean curvature can be calculated from $H = \frac{1}{n} h_{ij} g^{ji}$, where we use the Einstein summation convention, and $(g^{ij}) = (g_{ij})^{-1}$.

For $n = 2$, which fits into our purpose, let us choose $\mathbf{f}(\mathbf{u}) = (\mathbf{u_1}, \mathbf{u_2}, \chi)$, where $\chi(u_1, u_2)$ is a function of interest. We have the first fundamental form:

$$(g_{ij}) = \begin{pmatrix} 1 + \chi_1^2 & \chi_1 \chi_2 \\ \chi_1 \chi_2 & 1 + \chi_2^2 \end{pmatrix}, \tag{3}$$

where $\chi_i = \frac{\partial \chi}{\partial u_i}, i = 1, 2$. The inverse matrix of (g_{ij}) is given by

$$(g^{ij}) = \frac{1}{g} \begin{pmatrix} 1 + \chi_2^2 & -\chi_1 \chi_2 \\ -\chi_1 \chi_2 & 1 + \chi_1^2 \end{pmatrix}, \tag{4}$$

where $g = \text{Det}(g_{ij}) = 1 + \chi_1^2 + \chi_2^2$ is the Gram determinant. The normal vector can be computed from Eq. (1)

$$\mathbf{N} = \frac{(-\chi_1, -\chi_2, 1)}{\sqrt{g}}, \tag{5}$$

The second fundamental form is given by $(h_{ij}) = \left(\frac{1}{\sqrt{g}} \chi_{u_i u_j} \right)$, i.e., the Hessian matrix of χ.

The explicit form for the mean curvature operator can be written as

$$H = \frac{1}{2g}(h_{11} g_{22} + h_{22} g_{11} - 2 h_{12} g_{12}) \tag{6}$$

$$= \frac{1}{2} \left[\frac{\partial}{\partial u_1} \left(\frac{\chi_1}{\sqrt{g}} \right) + \frac{\partial}{\partial u_2} \left(\frac{\chi_2}{\sqrt{g}} \right) \right]. \tag{7}$$

In Section II.C.2, we show that the mean curvature operator can be expressed in a (3D) formulation.

II.B Solvation free energy functionals

This subsection presents a few solvation models and establishes the notations for the further development of differential geometry based solvation analysis. A polar solvation model is described before a nonpolar solvation model is given. The total solvation free energy functional is designed as the combination of the polar and nonpolar components.

II.B.1 Polar solvation functional

As illustrated in Fig. 1 above, the polar solvation energy is generally associated with a difference in charging free energies in vacuum and solvent. The origin of polar solvation energy is electrostatic interactions, which are of long range in nature and ubiquitous for any system of charged or polar molecules.

In general, biomolecules are very polarizable and can be highly charged. Therefore, according to electrodynamics, both electric field $\mathbf{E}$ and electric displacement $\mathbf{D}$ are important quantities for describing biomolecules. However, it is a convention in biophysics to only deal with the electric field in many force field models. As such, the polarization effects of neutral biomolecules are described as explicit

partial point charges associated with atoms. This approach is simple and systematic, and provides a reasonable approximation to a system without a strong external field, rapidly changing electric current and external magnetic field. In fact, if there is no external magnetic field and moving electric filed, the effects of magnetic field $\mathbf{H}$, magnetic displacement $\mathbf{B}$ and magnetic displacement are normally neglected in describing biomolecular systems.

The free energy functional of the electrostatic system was given by Sharp and Honig,[183] and Gilson et al.[86] A sharp solvent-solute interface is assumed in their free energy expression

$$G_{\rm p} = \int_{\Omega} \left(\lambda_m \rho_m \phi - \frac{1}{2}\epsilon|\nabla\phi|^2 - k_B T \lambda_s \sum_{i=1}^{N_c} c_i \left(e^{-\phi q_i/k_B T} - 1 \right) \right) d\mathbf{r} \tag{8}$$

where Ω denotes the whole computational domain, ϕ is the electrostatic potential, k_B is the Boltzmann constant, T is the temperature, c_j is the bulk concentration of jth ionic species, N_c is the number of ionic species, and $\rho_m(\mathbf{x}, \mathbf{z}) = \sum_j^{N_m} Q_j \delta(\mathbf{x} - \mathbf{z}_j)$ is the canonical density of molecular free charges, with Q_j being partial charges on (discrete) atoms and N_m is the number of charged particles. Here, the permittivity $\epsilon(\mathbf{r})$ (also called dielectric coefficient) and the ionic function $\lambda_m(\mathbf{r})$ and $\lambda_s(\mathbf{r})$ are defined as[6,82,131]

$$\epsilon(\mathbf{r}) = \epsilon_{\mathbf{m}}\lambda_{\mathbf{m}} + \epsilon_{\mathbf{s}}\lambda_{\mathbf{s}} \tag{9}$$

and

$$\lambda_m(\mathbf{r}) = \left\{ \begin{array}{ll} 1 & \mathbf{r} \in \Omega_m \\ 0 & \mathbf{r} \in \Omega_s \end{array} \right. \quad , \quad \lambda_s(\mathbf{r}) = \left\{ \begin{array}{ll} 0 & \mathbf{r} \in \Omega_m \\ 1 & \mathbf{r} \in \Omega_s \end{array} \right. \tag{10}$$

where, the computational domain is divided into two subdomains, $\Omega = \Omega_m \cup \Omega_s$, with Ω_m and Ω_s, denoting the solute and solvent accessible regions, respectively. The domains Ω_m and Ω_s are separated by an interface Γ. Here, $\epsilon_m = \epsilon_0 \varepsilon_m$ and $\epsilon_s = \epsilon_0 \varepsilon_s$ are the permittivities of the macromolecule and the solvent, respectively, where ϵ_0 is the permittivity of vacuum and ε_α ($\alpha = m, s$) are relative permittivities. We treat ε_α as constants. Note that in the class PB theory, these functions explicitly depend only on the radii of the solute[6,82] — they do not depend on Γ. However, in the present theory, these functions only implicitly depend on the radii of the solute. They depend explicitly on the interface Γ, which in turn, depends on the total energy functional.

The standard PB equation[86,183] can be derived by the variation of the electrostatic energy functional Eq. (8). The PB theory has a few well-known limitations. First, most implicit solvent models assume linear and local solvent response. However, nonlinear solvent response (usually through dielectric saturation or electrostriction) can be important in regions of strong electric field such as the regions near highly charged ions, biomolecules, and other interfaces.[71,182,216] Nonlocal solvent response, which generally describes the finite non-zero size of water and its unique hydrogen bonding with solute and other solvent molecules, can be crucial in accurately describing the orientation of water at biomolecular interfaces,[34] the solvation of cations from anions, and the solvation of asymmetric charge distributions.[142] Additionally, the PB theory utilizes the mean-field treatment for ions, which assumes that each ion experiences only the average influence of the other ions in solution. Such averaging precludes the detailed ion-ion interaction including the Coulombic interactions of ions and repulsive and attractive pairing. It thereby keeps us from the important analysis of correlations and fluctuations in the solutions with divalent and multivalent ions surrounding highly-charged molecules such as nucleic acids.[41,50,176,202,203] Finally, as implied by the above limitations, the PB theory neglects the detailed ion-solvent interactions and eliminates the differences between ions species in solutions which can be important in biophysical modeling. However, these limitations are not unique to the PB and apply to most other implicit solvent models. Furthermore, new implicit solvent models[5,50,147,161,202] and hybrid treatments[11,115,145,153,211] have been proposed in the literature to address these limitations and thereby extend the applicability of the PB theory while preserving some of its computational efficiency through pre-averaging solvent and ion response.

II.B.2 Nonpolar solvation functional

Poisson-Boltzmann methods provide *polar* solvation energies and therefore must be complemented by *nonpolar* solvation models to provide a complete view of solvent-solute interactions. As illustrated in Fig. 1, nonpolar solvation is generally associated with the insertion of the uncharged solute into solvent. There are many nonpolar solvation models available. The most commonly used one is the scaled particle theory (SPT)[164,194] which includes the energy of surface tension effect and the mechanical work of immersing a particle into the solvent. Recent work by Levy, Gallicchio, and others[79–81,118,214] has demonstrated the importance of nonpolar solvent models which include treatment of attractive solute-solvent dispersion terms (#5 in Fig. 1) as well as models of solvent-solvent repulsive interactions (#4 in Fig. 1), in addition to both area and volume contributions.[214] In the present work, we use the following model for nonpolar solvation free energies[214]

$$G_{\mathrm{np}} = \gamma(\mathrm{Area}) + p(\mathrm{Vol}) + \int_{\Omega_s} \rho_s U^{\mathrm{vdW}} d\mathbf{r}, \tag{11}$$

where γ is the surface tension, Area is the solvent-excluded area of the solute, p is the hydrodynamic pressure, Vol is the solvent-excluded volume of the solute, ρ_s is the solvent density, Ω_s denotes the solvent accessible region, and U^{vdW} is the solvent-solute van der Waals (vdW) interaction potential. The first two terms in Eq. (11) are those from the SPT model.[164,194] In general, U^{vdW} can be obtained by the sum of the interaction of individual atoms in Ω_m with the solvent continuum in Ω_s under the assumption that the nonpolar solute-solvent potential is pairwise: $U^{\mathrm{vdW}} = \sum_i V_i^{\mathrm{vdW}}$. This model of nonpolar solvation has been demonstrated by us to give good agreement with explicit solvent solvation forces on proteins[214] and RNA hairpins.[63] Work by Levy and co-workers has demonstrated the good performance of a similar model.[79–81,118]

In the present work, we further allow the solvent density ρ_s to be a function of position in general. In particular, we split the solvent density ρ_s into the sum of atomic or ionic density distribution functions $\rho_s = \sum_i \rho_{s,i}$. The distribution of an individual solvent component can be computed by integral equations or other approaches, such as Monte Carlo and generalized Langevin equation.[20,77,210] This design of solvent density allows us to recover the nonlinear and nonlocal effects of the solvent-solute interactions.

II.B.3 Total free energy functional of solvation

The electrostatic free energy functional is complemented by nonpolar free energy functional to give the total free energy functional of solvation for biomolecules at equilibrium

$$
\begin{aligned}
G_{\mathrm{full}} &= \gamma(\mathrm{Area}) + p(\mathrm{Vol}) + \int_{\Omega_s} \rho_s U^{\mathrm{vdW}} d\mathbf{r} \\
&+ \int_{\Omega_m} \left(\rho_m \phi - \frac{\epsilon_m}{2} |\nabla \phi|^2 \right) d\mathbf{r} - \int_{\Omega_s} \left(\frac{\epsilon_s}{2} |\nabla \phi|^2 + k_B T \sum_{i=1}^{N_c} c_i \left(e^{-\phi q_i / k_B T} - 1 \right) \right) d\mathbf{r},
\end{aligned} \tag{12}
$$

where we have used the coefficient definitions provided in Eqs. 9 and 10 to simplify the integrals. This total free energy functional might be subject to a variety of corrections and modifications. However, it is designed to maintain the computational efficiency of the implicit solvent models, while effectively addressing a number of major concerns in the implicit solvent theory. First, it provides atomic details of solute-solvent interactions to describe solvent behavior in situations where nonlinear and nonlocal solvent responses to the solute are important.[1,2,4,8,28,34,38,49,66–68,74,76,97,98,105,113,116,141,143,168,187,198,199,205,214] Additionally, as shown in the next subsection, the associated solvation model allows the solvent-solute interface to vary according to the minimization of the total free energy functional, which removes the *ad hoc* nature of prefixed surface definitions in the current practice and the associated controversy in choosing surfaces.[62,64]

II.C Lagrangian formulation of the solvation model

The total free energy functional (12) is an important component of the present differential geometry based solvation model. However, it does not provide a protocol for practical solvation analysis. This subsection describes the variation principle which leads to desirable governing equations for the surface formation and evolution, and for the evaluation of the electrostatic potential.

II.C.1 Surface variation

In our previous minimal molecular surface (MMS) model,[16,18] the surface variation was accomplished via the Euler-Lagrange equation in the Eulerian representation. In the present Lagrangian representation, we perform the minimization of G_{full} on manifold Ξ with respect to the solvent-solute interface Γ. In the spirit of differential geometry, the interface can be represented as a closed surface in the 3D Euclidean space and denoted as $\Gamma(u_1, u_2)$, which depends on the two real parameters u_1 and u_2. The solute region, $\Omega_m(\Gamma)$ and the solvent region, $\Omega_s(\Gamma)$ can be regarded as functions of $\Gamma(u_1, u_2)$. We use $\frac{\delta(\cdot)}{\delta\Gamma}$ to denote the first variation of $(\cdot)$ with respect to surface definition Γ,

$$
\begin{aligned}
\frac{\delta G_{\text{full}}}{\delta\Gamma} = {} & \frac{\delta}{\delta\Gamma}\left[\gamma(\text{Area}) + p(\text{Vol}) + \int_{\Omega_s}\rho_s U^{\text{vdW}}d\mathbf{r} + \int_{\Omega_m}\rho_m\phi d\mathbf{r}\right. \\
& \left. -\frac{1}{2}\left(\int_{\Omega_s}\epsilon_s|\nabla\phi|^2 d\mathbf{r} + \int_{\Omega_m}\epsilon_m|\nabla\phi|^2 d\mathbf{r}\right) - \int_{\Omega_s}k_B T\sum_{i=1}^{N_c}c_i\left(e^{-\phi q_i/k_B T} - 1\right)d\mathbf{r}\right].
\end{aligned}
\tag{13}
$$

We set $\frac{\delta G_{\text{full}}}{\delta\Gamma} = 0$ to construct the governing equation that describes the optimized solvent-solute interface. To carry out this variation, we express the surface area and volume as the following integrals

$$
\text{Area} = \int_\Xi d\sigma \quad \text{and} \quad \text{Vol} = \int_{\Omega_m}d\mathbf{r},
\tag{14}
$$

where $d\sigma$ represents the infinitesimally small surface element on the solute-solvent interface. The complete first variation formula of G can be obtained by adding up the variation of each term from Eq. (13). To this end, we consider a surface element $\mathbf{f}(u_1, u_2)$ and its infinitesimal displacement in the normal direction

$$
\mathbf{f}^{(\varepsilon)}(u_1, u_2) := \mathbf{f}(u_1, u_2) + \varepsilon\varphi(u_1, u_2)\cdot\mathbf{N}(u_1, u_2)
\tag{15}
$$

where $\mathbf{N}$ is the outward unit normal direction and φ is an arbitrary C^2 function. In other words, we consider a one-parameter family $\mathbf{f}^{(\varepsilon)}$ of surface elements and the unperturbed surface element is a particular case, $\mathbf{f} = \mathbf{f}^{(0)}$. The tangent vectors of $\mathbf{f}^{(\varepsilon)}$ are given by

$$
\frac{\partial\mathbf{f}^{(\varepsilon)}}{\partial u_i} = \frac{\partial\mathbf{f}}{\partial u_i} + \varepsilon\frac{\partial\varphi}{\partial u_i}\mathbf{N} + \varepsilon\varphi\frac{\partial\mathbf{N}}{\partial u_i}.
\tag{16}
$$

To analyze the impact of the perturbation, we examine the first fundamental form of differentiable manifolds

$$
\begin{aligned}
g_{ij}^{(\varepsilon)} = {} & \left\langle\frac{\partial\mathbf{f}^{(\varepsilon)}}{\partial u_i}, \frac{\partial\mathbf{f}^{(\varepsilon)}}{\partial u_j}\right\rangle \\
= {} & g_{ij} + 2\varepsilon\varphi\left\langle\frac{\partial\mathbf{f}}{\partial u_i}, \frac{\partial\mathbf{N}}{\partial u_j}\right\rangle + \varepsilon^2\left(\varphi^2\left\langle\frac{\partial\mathbf{N}}{\partial u_i}, \frac{\partial\mathbf{N}}{\partial u_j}\right\rangle + \frac{\partial\varphi}{\partial u_i}\frac{\partial\varphi}{\partial u_j}\right) \\
= {} & g_{ij} - 2\varepsilon\varphi h_{ij} + O(\varepsilon^2).
\end{aligned}
\tag{17}
$$

We therefore have

$$
\left.\frac{\partial g_{ij}^{(\varepsilon)}}{\partial\varepsilon}\right|_{\varepsilon=0} = -2\varphi h_{ij}.
\tag{18}
$$

By virtue of surface elements $f^{(\varepsilon)}$ and the first fundamental form, we can carry out the surface variation of the area as follows

$$
\begin{aligned}
\frac{\delta A}{\delta \Gamma} &= \frac{\delta}{\delta \Gamma}\left(\int_{\Xi} d\sigma\right) \\
&= \frac{\delta}{\delta \Gamma}\left(\int_{U} \sqrt{g}\, du_1 du_2\right) \\
&= \left.\frac{\partial}{\partial \varepsilon}\right|_{\varepsilon=0}\left(\int_{U} \sqrt{g^{(\varepsilon)}}\, du_1 du_2\right) \\
&= \left(\int_{U} \left.\frac{\partial}{\partial \varepsilon}\right|_{\varepsilon=0} \sqrt{g^{(\varepsilon)}}\, du_1 du_2\right) \\
&= \int_{U} \frac{1}{2\sqrt{g}}\left(g_{22}\left.\frac{\partial g_{11}^{(\varepsilon)}}{\partial \varepsilon}\right|_{\varepsilon=0} + g_{11}\left.\frac{\partial g_{22}^{(\varepsilon)}}{\partial \varepsilon}\right|_{\varepsilon=0} - 2g_{12}\left.\frac{\partial g_{12}^{(\varepsilon)}}{\partial \varepsilon}\right|_{\varepsilon=0}\right) du_1 du_2 \\
&= -\int_{U} \varphi \frac{1}{g}\left(h_{11}g_{22} + h_{22}g_{11} - 2h_{12}g_{12}\right) \sqrt{g}\, du_1 du_2 \\
&= -\int_{U} \varphi 2H \sqrt{g}\, du_1 du_2 \\
&= -\int_{\Xi} \varphi 2H\, d\sigma,
\end{aligned}
\tag{19}
$$

where g is the Gram determinant, $g = \mathrm{Det}(g_{ij}) = g_{11}g_{22} - g_{12}^2$ and H the mean curvature $H = \frac{1}{2g}(h_{11}g_{22} + h_{22}g_{11} - 2h_{12}g_{12})$, where g_{ij} and h_{ij} are defined in Section II.A.

The first variation of the volume enclosed by the manifold Ξ is derived as follows. We first express the volume enclosed by the surface element $\mathbf{f}^{(\varepsilon)}$ as a Taylor expansion in terms of ε

$$
\mathrm{Vol}(\mathbf{f}^{(\varepsilon)}) = \mathrm{Vol}(\mathbf{f}) + \varepsilon \frac{\delta \mathrm{Vol}}{\delta \Gamma} + O(\varepsilon^2).
\tag{20}
$$

As shown in the above calculation, we can pursue the volume variation with respect to Γ by means of the variation with respect to ε

$$
\frac{\delta \mathrm{Vol}}{\delta \Gamma} = \left.\frac{\partial \mathrm{Vol}(\mathbf{f}^{(\varepsilon)})}{\partial \varepsilon}\right|_{\varepsilon=0} = \left.\frac{\partial(\mathrm{Vol}(\mathbf{f}^{(\varepsilon)}) - \mathrm{Vol}(\mathbf{f}))}{\partial \varepsilon}\right|_{\varepsilon=0}.
\tag{21}
$$

It follows[21]

$$
\begin{aligned}
\frac{\delta \mathrm{Vol}}{\delta \Gamma} &= \left.\frac{\partial(\mathrm{Vol}(f^{(\varepsilon)}) - \mathrm{Vol}(f))}{\partial \varepsilon}\right|_{\varepsilon=0} \\
&= \left.\frac{\partial \int_0^{\varepsilon} \int_{U} \sqrt{\mathrm{Det} J}\, du_1 du_2 d\tau}{\partial \varepsilon}\right|_{\varepsilon=0} \\
&= \left.\int_{U} \sqrt{\mathrm{Det} J}\, du_1 du_2\right|_{\tau=\varepsilon=0} \\
&= \int_{U} \varphi \sqrt{g}\, du_1 du_2 \\
&= \int_{\Xi} \varphi\, d\sigma,
\end{aligned}
\tag{22}
$$

13

where matrix J is defined as

$$J = \begin{pmatrix} \left\langle \frac{\partial \mathbf{f}^{(\tau)}}{\partial u_1}, \frac{\partial \mathbf{f}^{(\tau)}}{\partial u_1} \right\rangle & \left\langle \frac{\partial \mathbf{f}^{(\tau)}}{\partial u_1}, \frac{\partial \mathbf{f}^{(\tau)}}{\partial u_2} \right\rangle & \left\langle \frac{\partial \mathbf{f}^{(\tau)}}{\partial u_1}, \frac{\partial \mathbf{f}^{(\tau)}}{\partial \tau} \right\rangle \\ \left\langle \frac{\partial \mathbf{f}^{(\tau)}}{\partial u_2}, \frac{\partial \mathbf{f}^{(\tau)}}{\partial u_1} \right\rangle & \left\langle \frac{\partial \mathbf{f}^{(\tau)}}{\partial u_2}, \frac{\partial \mathbf{f}^{(\tau)}}{\partial u_2} \right\rangle & \left\langle \frac{\partial \mathbf{f}^{(\tau)}}{\partial u_2}, \frac{\partial \mathbf{f}^{(\tau)}}{\partial \tau} \right\rangle \\ \left\langle \frac{\partial \mathbf{f}^{(\tau)}}{\partial \tau}, \frac{\partial \mathbf{f}^{(\tau)}}{\partial u_1} \right\rangle & \left\langle \frac{\partial \mathbf{f}^{(\tau)}}{\partial \tau}, \frac{\partial \mathbf{f}^{(\tau)}}{\partial u_2} \right\rangle & \left\langle \frac{\partial \mathbf{f}^{(\tau)}}{\partial \tau}, \frac{\partial \mathbf{f}^{(\tau)}}{\partial \tau} \right\rangle \end{pmatrix}, \tag{23}$$

and similarly, $\mathbf{f}^{(\tau)} = \mathbf{f} + \tau\varphi \cdot \mathbf{N}, \quad \tau \in (0, \varepsilon)$. We have carried out the calculation of inner products

$$\left\langle \frac{\partial \mathbf{f}^{(\tau)}}{\partial u_i}, \frac{\partial \mathbf{f}^{(\tau)}}{\partial \tau} \right\rangle \Bigg|_{\tau=0} = \left\langle \frac{\partial \mathbf{f}^{(\tau)}}{\partial u_i}, \varphi\mathbf{N} \right\rangle \Bigg|_{\tau=0} = 0, \tag{24}$$

where $\left\langle \frac{\partial \mathbf{f}^{(\tau)}}{\partial u_i}, \varphi\mathbf{N} \right\rangle$ vanishes since $\frac{\partial \mathbf{f}^{(\tau)}}{\partial u_i}$ and $\mathbf{N}$ are orthogonal to each other. Moreover, we have

$$\left\langle \frac{\partial \mathbf{f}^{(\tau)}}{\partial \tau}, \frac{\partial \mathbf{f}^{(\tau)}}{\partial \tau} \right\rangle = \varphi^2, \tag{25}$$

where we use the fact that $\frac{\partial \mathbf{f}^{(\tau)}}{\partial \tau} = \varphi\mathbf{N}$. Therefore, we can compute the determinant of the J matrix as

$$\text{Det} J|_{\tau=0} = \text{Det} \begin{pmatrix} \left\langle \frac{\partial \mathbf{f}}{\partial u_1}, \frac{\partial \mathbf{f}}{\partial u_1} \right\rangle & \left\langle \frac{\partial \mathbf{f}}{\partial u_1}, \frac{\partial \mathbf{f}}{\partial u_2} \right\rangle & 0 \\ \left\langle \frac{\partial \mathbf{f}}{\partial u_2}, \frac{\partial \mathbf{f}}{\partial u_1} \right\rangle & \left\langle \frac{\partial \mathbf{f}}{\partial u_2}, \frac{\partial \mathbf{f}}{\partial u_2} \right\rangle & 0 \\ 0 & 0 & \varphi^2 \end{pmatrix} = \varphi^2 g. \tag{26}$$

Moreover, the above derivation process can be extended to the first variation of a general volume integral $\int_{\Omega_m} F(\mathbf{r})d\mathbf{r}$.

$$\begin{aligned} \frac{\delta \left(\int_{\Omega_m} F d\mathbf{r} \right)}{\delta \Gamma} &= \frac{\partial \int_0^\varepsilon \int_U F(u_1, u_2, \tau)\sqrt{\text{Det} J} du_1 du_2 d\tau}{\partial \varepsilon} \Bigg|_{\varepsilon=0} \\ &= \int_\Xi F(u_1, u_2)\varphi d\sigma \end{aligned} \tag{27}$$

where F represents a general integrable function of u_1 and u_2, and is defined in the whole domain. Similar to the volume variation, we end up with a surface integral.

Furthermore, because $\int_\Omega F d\mathbf{r}$ is independent of the surface variation, we have

$$\frac{\delta(\int_\Omega F d\mathbf{r})}{\delta \Gamma} = 0. \tag{28}$$

Then, it follows that

$$\frac{\delta \left(\int_{\Omega_s} F d\mathbf{r} \right)}{\delta \Gamma} = \frac{\delta(\int_\Omega F d\mathbf{r} - \int_{\Omega_m} F d\mathbf{r})}{\delta \Gamma} = -\int_\Xi F\varphi d\sigma. \tag{29}$$

Therefore, the first variation of all other volume integration terms in Eq. (13) can be attained by replacing F with appropriate integrands in Eq. (27) and Eq. (29)

$$\frac{\delta \left(\int_{\Omega_m} \rho_m \phi d\mathbf{r} \right)}{\delta \Gamma} = \int_\Xi \rho_m \phi d\sigma, \tag{30}$$

$$\frac{\delta \left(\int_{\Omega_s} \epsilon_s |\nabla\phi|^2 d\mathbf{r} \right)}{\delta \Gamma} = -\int_\Xi \epsilon_s |\nabla\phi|^2 \varphi d\sigma, \tag{31}$$

14

$$\frac{\delta \left(\int_{\Omega_m} \epsilon_m |\nabla \phi|^2 d\mathbf{r} \right)}{\delta \Gamma} = \int_{\Xi} \epsilon_m |\nabla \phi|^2 \varphi d\sigma, \tag{32}$$

$$\frac{\delta \left(\int_{\Omega_s} \rho_s U^{\mathrm{vdW}} d\mathbf{r} \right)}{\delta \Gamma} = - \int_{\Xi} \rho_s U^{\mathrm{vdW}} \varphi d\sigma \tag{33}$$

and

$$\frac{\delta \left(\int_{\Omega_s} k_B T \sum_{i=1}^{N_c} c_i \left(e^{-\phi q_i / k_B T} - 1 \right) d\mathbf{r} \right)}{\delta \Gamma} \tag{34}$$

$$= - \int_{\Xi} k_B T \sum_{i=1}^{N_c} c_i \left(e^{-\phi q_i / k_B T} - 1 \right) \varphi d\sigma,$$

where $\nabla \phi$ on the surface represents the first derivative of potential ϕ. These expressions have different signs due to the flux continuity condition in the Poisson-Boltzmann equation when the discontinuous dielectric constant is applied.

Substituting Eqs. (19), (22), (30) (31), (32), (33), (34) into Eq. (13) yields

$$\frac{\delta G_{\mathrm{full}}}{\delta \Gamma} = \int_{\Xi} \left[-2\gamma H + p - \rho_s U^{\mathrm{vdW}} + \rho_m \phi + \frac{1}{2} \epsilon_s |\nabla \phi|^2 - \frac{1}{2} \epsilon_m |\nabla \phi|^2 \right. \tag{35}$$

$$\left. + k_B T \sum_{i=1}^{N_c} c_i \left(e^{-\phi q_i / k_B T} - 1 \right) \right] \varphi d\sigma = 0.$$

Since φ is an arbitrary function, the following condition must be satisfied for each point on the optimized interface

$$W_n \equiv -2\gamma H + p - \rho_s U^{\mathrm{vdW}} + \rho_m \phi + \frac{1}{2} \epsilon_s |\nabla \phi|^2 - \frac{1}{2} \epsilon_m |\nabla \phi|^2 \tag{36}$$

$$+ k_B T \sum_{i=1}^{N_c} c_i \left(e^{-\phi q_i / k_B T} - 1 \right)$$

$$= 0$$

It is noted that this condition was also obtained in our earlier work, but was derived in the Eulerian representation using different mathematical techniques.[42,221]

II.C.2   Governing equations

The directional derivative of solvation free energy functional G in the direction of a normal variation φ can be expressed as

$$D_\varphi G_{\mathrm{full}}(\mathbf{f}) = \left. \frac{\partial G_{\mathrm{full}}(\mathbf{f}^{(\varepsilon)})}{\partial \varepsilon} \right|_{\varepsilon=0} = \int_{\Xi} W_n \varphi d\sigma. \tag{37}$$

If we choose $\varphi(u_1, u_2) = -W_n$, then $D_\varphi G_{\mathrm{full}}(\mathbf{f}) = -\int_{\Xi} W_n^2 d\sigma \leq 0$. This means that the total free energy decreases along the normal direction when $\varphi(u_1, u_2) = -W_n$ until it reaches a local minimal. Therefore the evolution $\mathbf{f}^{(\varepsilon)} = \mathbf{f} - \varepsilon W_n \mathbf{N}$ leads to a steady state and associated solvent-solute interface with strictly smaller energy. This analysis motivates the following potential driven geometric flow equation for the optimization of the solute-solvent interface

$$\frac{\partial \mathbf{X}}{\partial t} = -W_n \mathbf{N}, \tag{38}$$

where $\mathbf{X} \in \Xi \subset \mathbb{R}^3$ is a position vector on the evolving manifold Ξ. Equation (38) is a Lagrange formulation of generalized geometric flows and its structure has been discussed in our earlier work.[15] This

approach is computationally efficient but may have difficulties in handling topological changes during the biomolecule surface evolution. Numerical schemes for the solution of geometric flow equations will be described in Section III.B.

The electrostatic potential ϕ is governed by the Poisson-Boltzmann equation for traditional continuum biomolecular electrostatics applications. In the present approach, the Poisson-Boltzmann equation can be easily derived from the variation of the full free energy functional in Eq. (12) with respect to the electrostatic potential ϕ for a fixed interface Γ via the Euler Lagrange equation[86, 183, 221]

$$\frac{\delta G_{\text{full}}}{\delta \phi} = 0 \Rightarrow \quad -\nabla \cdot (\epsilon(\mathbf{r})\nabla\phi) - \lambda_s(\mathbf{r}) \sum_{i=1}^{N_c} q_i c_i e^{-\phi q_i/k_B T} = \lambda_m \rho_m. \tag{39}$$

This Poisson-Boltzmann equation admits a sharp solvent-solute interface Γ and is quite different from the generalized Poisson-Boltzmann equation derived in our earlier work,[42, 221] which has an optimized smooth surface (OSS).

Note that the Poisson-Boltzmann equation (39) and the potential driven geometry flow equation (38) are fully coupled. The existence and the uniqueness of their solution under the biomolecular context can be an interesting mathematical issue. In practice, these two equations have to be solved in a self-consistent manner. This aspect is discussed in §III.B.3. The solution of the Poisson-Boltzmann equation is subject to the far field boundary condition, which in practice can be approximated by the Dirichlet type of boundary conditions commonly used in continuum electrostatic modeling (see Eq. (44)).

Assuming that there are only two mobile ion spices and all ions are univalent, we can treat them as positive and negative ions with charge $+e_c$ and $-e_c$, where e_c is the electron charge. Then the nonlinear Poisson-Boltzmann (NLPB) equation (39) becomes[82, 95]

$$-\nabla \cdot (\epsilon(\mathbf{r})\nabla\phi) + \overline{\kappa}^2(\mathbf{r}) \left(\frac{k_B T}{e_c} \right) \sinh \left(\frac{e_c \phi}{k_B T} \right) = \lambda_m \rho_m, \tag{40}$$

where $\overline{\kappa}$ is the modified Debye-Hückel screening function describing ion strength and is determined by

$$\overline{\kappa}^2 = \left(\frac{2\lambda_s N_a e_c^2}{1000 k_B T} I_s \right), \tag{41}$$

where N_a the Avogadro's number, and I_s the ion strength in the unit of mole. Numerically, when $T = 298$K, the value of $\overline{\kappa}^2$ can be obtained via $\overline{\kappa}^2 = 0.675365$ Å$^{-2} I_s$. Note that Debye-Hückel parameter $\overline{\kappa}$ can also be expressed as[86]

$$\overline{\kappa}^2 = \frac{\lambda_s}{k_B T} \sum_{i=1}^{N_c} c_i q_i^2. \tag{42}$$

Equations (41) and (42) are equivalent to each other via the following formula[95]

$$I_s = \frac{1}{2e_c^2} \sum_{i=1}^{N_c} c_i q_i^2 = \frac{1000M}{N_a}, \tag{43}$$

where M is the bulk concentration of ions in the unit of mole per cubic centimeter $\left(\frac{\text{mol}}{\text{cm}^3} \right)$ for both positive and negative ionic charges. Equation (40) is subject to the far-field boundary condition $\phi(\infty) = 0$. However, the Dirichlet boundary condition is used in practical computations

$$\phi(\mathbf{r}) = \sum_i \phi_i = \sum_{i=1}^{N_m} \frac{Q_i}{\epsilon_s |\mathbf{r} - \mathbf{r}_i|} e^{-\overline{\kappa}|\mathbf{r} - \mathbf{r}_i|/\epsilon_s} \quad \forall \mathbf{r} \in \partial\Omega, \tag{44}$$

where ϕ_i is the exact solution of a single ion in a homogeneous media. The linear superposition in Eq. (44) is very accurate if the macromolecule domain Ω_m is sufficiently away from the boundary $\partial\Omega$.

Let define a dimensionless potential u through $u = e_c \phi / k_B T$, one yields another formulation of the nonlinear PB equation in terms of u[36]

$$-\nabla \cdot (\epsilon(\mathbf{r}) \nabla u) + \overline{\kappa}^2(\mathbf{r}) \sinh(u) = \frac{e_c}{k_B T} \lambda_m \rho_m. \tag{45}$$

If the potential is very weak, i.e., $u \ll 1$, one can numerically solve the following linearized PB (LPB) equation

$$-\nabla \cdot (\epsilon(\mathbf{r}) \nabla u) + \overline{\kappa}^2(\mathbf{r}) u(\mathbf{r}) = \frac{e_c}{k_B T} \lambda_m \rho_m. \tag{46}$$

Note that in the Poisson-Boltzmann theory, there are two unit conventions in the literature that differs by a factor of 4π. Specifically, the convention used by Sharp and Honig,[184] and in some of our earlier work[36,82] has a factor of 4π in the Poisson-Boltzmann equation. Whereas, the convention used by Gilson et al.[86] and in our recent work[42,221] as well as the present derivation, the 4π factor does not appear. Therefore, care is needed in the comparison of the electrostatic potentials computed by these two conventions.

III   Method and algorithm

This section discusses the solution strategies for the coupled potential driven geometric flow and the Poisson-Boltzmann equation.

III.A   Interconversion between the Lagrangian and Eulerian representations

The generalized geometric flow equation (38) is in the Lagrangian representation which is well suited for boundary element or finite element type of methods. Although this Lagrangian formulation of geometry flow models is relatively easy to implement in many applications, such as surface smoothing, it can lead to computational difficulties in the case where there are topological changes, such as surface breaking or merging. These difficulties origin from the fact of singularity development on the manifold which is supposed to be smooth and differentiable. These topological changes commonly occur in biomolecular surface constructions and molecular dynamics applications. One way to overcome these obstacles is to use the Eulerian formulation.[15–18,223] The essential idea of resolving the difficulty of a "singular manifold" or non-smooth surface is to embed the problem in a higher dimensional space such that the embedded function is smooth and differentiable. Another way to avoid the difficulty of singular manifolds is to use a hybrid Eulerian-Lagrangian approach for biomolecular surface generation. In such a hybrid approach, the surface evolution is carried out most in the Lagrangian representation, but is temporally switched to the Eulerian representation whenever there is a singularity development on the manifold. In the rest of this subsection, we discuss computational tools for the interconversion between the Lagrangian and Eulerian representations.

III.A.1   Embedding the Lagrangian dynamics into the Eulerian representation

To embed a Lagrangian operator into its Eulerian representation, we introduce arbitrary hypersurface function $S(\mathbf{r})$ with $\mathbf{r} \in \mathbb{R}^3$. The earlier function $\chi(u_1, u_2)$ can be obtained by solving $S = 0$. For example, if $S = X_0 x^2 + Y_0 y^3 + Z_0 z + D_0$, where, X_0, Y_0 and Z_0 are constants, and $z_0 \neq 0$, then one can set

$$\chi(t) = z = -x_0 x^2 - y_0 y^3 - d_0, \quad x_0 = \frac{X_0}{Z_0}, y_0 = \frac{Y_0}{Z_0}, d_0 = \frac{D_0}{Z_0}. \tag{47}$$

Via this example, it is easy to verify that the unit norm vector defined in Eq. (5) can also be expressed in term of S

$$\mathbf{N} = \frac{(-\chi_1, -\chi_2, 1)}{\sqrt{g}} = \frac{\nabla S}{\|\nabla S\|}. \tag{48}$$

Then the desired surface can be represented as a set of points with a constant value of function S

$$\Xi = \{\mathbf{r} | S(\mathbf{r}) = L\} \tag{49}$$

where L is an isosurface value. By the chain rule

$$
\begin{aligned}
\frac{\partial S}{\partial t} &= \frac{\partial S}{\partial \mathbf{X}} \cdot \frac{\partial \mathbf{X}}{\partial t} \\
&= \nabla S \cdot \frac{\partial \mathbf{X}}{\partial t} \\
&= -W_n \nabla S \cdot \mathbf{N},
\end{aligned}
\tag{50}
$$

where $\mathbf{X}$ is a 3D position vector confined to the manifold Ξ. Due to Eq. (48), one has

$$
\begin{aligned}
\frac{\partial S}{\partial t} &= -\|\nabla S\| W_n \\
&= \|\nabla S\| \left[2\gamma H - p + \rho_s U^{\text{vdW}} - \rho_m \phi - \frac{1}{2}\epsilon_s |\nabla \phi|^2 \right. \\
&\quad \left. + \frac{1}{2}\epsilon_m |\nabla \phi|^2 - k_B T \sum_{i=1}^{N_c} c_i \left(e^{-\phi q_i/k_B T} - 1 \right) \right]
\end{aligned}
\tag{51}
$$

where all terms should be expressed in terms of level surface function S. In particular, surface mean curvature H must be rewritten in terms of S. The explicit form of mean curvature (7) implies the equality $2H = \nabla \cdot \mathbf{N}$ which gives

$$
H = \frac{1}{2} \left[\frac{\partial}{\partial u_1} \left(\frac{\chi_1}{\sqrt{g}} \right) + \frac{\partial}{\partial u_2} \left(\frac{\chi_2}{\sqrt{g}} \right) \right] = \frac{1}{2} \nabla \cdot \left(\frac{\nabla S}{\|\nabla S\|} \right).
\tag{52}
$$

One can easily verify this relation by Eq. (47). Equation (52) connects the Lagrangian representation of the Laplace-Beltrami operator with its Eulerian representation. Eventually, the potential driven geometry flow equation in the Eulerian form is obtained for the optimized solvent-solute interface

$$
\begin{aligned}
\frac{\partial S}{\partial t} &= \|\nabla S\| \left[\nabla \cdot \left(\frac{\gamma \nabla S}{\|\nabla S\|} \right) - p + \rho_s U^{\text{vdW}} - \rho_m \phi - \frac{1}{2}\epsilon_s |\nabla \phi|^2 \right. \\
&\quad \left. + \frac{1}{2}\epsilon_m |\nabla \phi|^2 - k_B T \sum_{i=1}^{N_c} c_i \left(e^{-\phi q_i/k_B T} - 1 \right) \right] \\
&= \|\nabla S\| \left[\gamma \nabla \cdot \left(\frac{\nabla S}{\|\nabla S\|} \right) + V \right]
\end{aligned}
\tag{53}
$$

where

$$
V = -p + \rho_s U^{\text{vdW}} - \rho_m \phi - \frac{1}{2}\epsilon_s |\nabla \phi|^2 + \frac{1}{2}\epsilon_m |\nabla \phi|^2 - k_B T \sum_{i=1}^{N_c} c_i \left(e^{-\phi q_i/k_B T} - 1 \right).
\tag{54}
$$

Equation (53) is the same as the generalized geometric flow equation derived in our earlier work using the characteristic function and geometric measure theory.[42] This consistency lays the foundation for switches forwards and backwards between the Eulerian and Lagrangian representations and the development of hybrid methods for biomolecular surfaces. In fact, Eq. (53) has the same structure as that of our potential and curvature driven geometric flows and V is essentially the generalized potential defined in our earlier work.[15] Eq. (53) is subject to the similar boundary and initial conditions as those of geometric PDEs described in our earlier work.[15, 16, 18]

III.A.2 Transform from the Lagrangian representation to the Eulerian representation

Usually the Lagrangian representation of surfaces is expressed in the form of triangulations.[173] To convert the Lagrangian representation of surfaces into the Eulerian representation, specifically, a Cartesian grid, we need to register the set of intersecting points between the surface and the Cartesian mesh. For the purpose of computing the electrostatic potential from the Poisson-Boltzmann equation which admits

discontinuous coefficients across the solvent-solute interface, we have to calculate the norms at all of the intersecting points as well. A numerical algorithm for this Lagrangian-Eulerian transformation of molecular surfaces was developed by Zhou et al.,[237] although the original paper did not provide implementation details.

We first set up a plane equation for each triangle on the molecular surface. For each plane equation, we compute all the intersection points between plane and the Cartesian mesh. For this set of intersecting points, we further record the subset that are located within the triangle. For this subset of intersecting points, we finally compute their norms as well by the second order finite difference scheme.[237] This algorithm has been extensively tested in our previous work.[18,82,230,237]

III.A.3 Transform from the Eulerian representation to the Lagrangian representation

Once the hypersurface function $S(x, y, z, T)$, where T is the stopping time, is obtained from the potential driven geometric flow equation (53) the solvent-solute interface can be extracted easily as an isosurface, $S(x, y, z, T) = L$, where isosurface value $L = (1 - \delta)S_0$. Here S_0 is set as the initial amplitude in geometry flow equation and $1 > \delta > 0$. In our earlier work,[16,18] we have chosen $S_0 = 1000$ and a small δ. Recently, in our differential geometry based multiscale models,[221] we have designated S as characteristic function of the solute and chosen $0 \leq S \leq 1$. There is no need to specify L in such a formulation. In the present work, we choose $L = S_{\max}/2$, where $S_{\max}$ is the maximum of S. This choice is computationally stable and delivers correct MMSs, when the potential term is absent. It is to point out that S here is quite different from the S used in our Eulerian formulation.[42] In the present work, S only serves as a hypersurface function for evolving and extracting the solvent-solute interface and can take any real value. Numerically, isosurface extraction can be done by existing software such as MATLAB. However, for further electrostatic analysis, we need a Cartesian representation of the interface locations and the associated norm values. Therefore, we construct a stand-alone algorithm to extract interface information. To this end, the marching cubes method is adopted.[128] For a given grid partition, the marching cubes algorithm simply deals with a local meshing problem by processing each cell or cube independently. Each vertex of a cube can be either greater or less than the threshold value L, giving 256 different scenarios. In considering the symmetry and complementarity, there are only 15 canonical configurations in each cell needed to be addressed for the local meshing.[59,128] A look-up table is a quite efficient local triangulation or Cartesian algorithm. The marching cubes method can be modified in many ways to improve the accuracy, efficiency, robustness, and topological correctness. Auxiliary binary tree structures are typically employed in the range-space approaches, such as kd-tree method and interval tree method, to speed up the marching cubes method. For a structured grid dataset, geometric searching methods exploiting spatial coherence can be simpler and more efficient than the range space approaches.

To implement this scheme, first all points inside or outside the surface must be identified according to S value in the Cartesian grid domain. The surface must intersect those cube edges where one vertex is outside and the other is inside the surface. Therefore the surface intersection points and their normal directions can be approximated by linear interpolation. For instant, to compute an intersection point $\mathbf{r}_o$ between an inside grid point $\mathbf{r}_1$ with value S_1 and an outside grid point $\mathbf{r}_2$ with value S_2, the distance d between $\mathbf{r}_o$ and $\mathbf{r}_1$ is calculated by

$$
\begin{aligned}
L &= S_1 * (1 - d) + S_2 * d \\
d &= \frac{S_1 - L}{S_1 - S_2}
\end{aligned}
\tag{55}
$$

where L is the isosurface function value. Obviously, with known positions $\mathbf{r}_1$ and $\mathbf{r}_2$, distance d determines the position of the intersection point $\mathbf{r}_o$. To calculate the norm vector at $\mathbf{r}_o$, we need to compute the normal vectors at $\mathbf{r}_1$ and $\mathbf{r}_2$. In general, the normal direction of a grid point (x_i, y_j, z_k) can be estimated

by

$$n_x(x_i, y_j, z_k) = \frac{S_{i+1,j,k} - S_{i-1,j,k}}{2\Delta x} \tag{56}$$

$$n_y(x_i, y_j, z_k) = \frac{S_{i,j+1,k} - S_{i,j-1,k}}{2\Delta y}$$

$$n_z(x_i, y_j, z_k) = \frac{S_{i,j,k+1} - S_{i,j,k-1}}{2\Delta z}$$

$$\mathbf{n} = (n_x, n_y, n_z)$$

where n_x, n_y and n_z are the x, y and z components of the norm, respectively. Thus, the norm at the intersecting point $\mathbf{r}_o$, denoted as $\mathbf{n}_o$, can be interpolated through $\mathbf{n}_1$ and $\mathbf{n}_2$, the norms of $\mathbf{r}_1$ and $\mathbf{r}_2$, respectively

$$\mathbf{n}_o = (1-d)\mathbf{n}_1 + d\mathbf{n}_2. \tag{57}$$

Clearly, the choice of $L = S_{\max}/2$ offers the best computational accuracy and stability. The unit norm $\mathbf{N}_o$ at the intersecting point can be easily computed as $\mathbf{N}_o = \frac{\mathbf{n}_o}{\|\mathbf{n}_o\|}$. This algorithm is used in our calculation of unit norms at the intersecting points. Obviously, higher-order algorithms can be easily constructed when they are needed.

III.A.4   Numerical surface integral and volume integral in the Eulerian representation

Very often, we need to accurately carry out surface integration and volume integration in the Eulerian representation. The surface integral of a density function f can be approximated by[189]

$$\int_{\Xi} f(x,y,z)d\sigma = \int_{\Omega} f(x,y,z)\delta(d(x,y,z))d\mathbf{r} \approx \sum_{i,j,k} f(x_i, y_j, z_k)\tilde{\delta}_{i,j,k}h^3 \tag{58}$$

where (x_i, y_j, z_k) is the coordinate of grid point (i, j, k), $d(x, y, z)$ is the distance of a point (x, y, z) defined in Ω from the interface Γ, h is the uniform grid size, and $f(x, y, z)$ is the surface density function defined on Γ. The delta function $\tilde{\delta}_{i,j,k}$ is given by

$$\tilde{\delta}_{i,j,k} = \tilde{\delta}_{i,j,k}^{(+x)} + \tilde{\delta}_{i,j,k}^{(-x)} + \tilde{\delta}_{i,j,k}^{(+y)} + \tilde{\delta}_{i,j,k}^{(-y)} + \tilde{\delta}_{i,j,k}^{(+z)} + \tilde{\delta}_{i,j,k}^{(-z)} \tag{59}$$

where $\tilde{\delta}_{i,j,k}^{(\pm\alpha)}, (\alpha = x, y, z)$ are discrete delta functions.[189] To carry out integration exactly on the interface, we use the following discrete surface integration formula[83]

$$\int_{\Xi} f(x,y,z)d\sigma \approx \sum_{(i,j,k)\in I} \left(f(x_o, y_j, z_k)\frac{|n_x|}{h} + f(x_i, y_o, z_k)\frac{|n_y|}{h} + f(x_i, y_j, z_o)\frac{|n_z|}{h} \right) h^3 \tag{60}$$

where (x_o, y_j, z_k) is the intersecting point of the interface and the x meshline that passes through (i, j, k), and n_x is the x component of the normal vector at (x_o, y_j, z_k). Similar relations exist between (x_i, y_o, z_k) and n_y, and (x_i, y_j, z_o) and n_z. Since Eq. (60) has already taken into account the contribution from irregular grid points outside the interface, the summation is restricted to I, the set of irregular grid points inside or on the interface.[83] The derivation of Eq. (60) is lengthy and is omitted here but it can be seen elsewhere.[83] The surface area can be calculated by setting $f = 1$ in Eq. (60). The error of the surface integration depends on the grid resolution and was observed to be approximately second-order convergence.[83]

The volume integral of the density function f can be simply approximated by[83]

$$\int_{\Omega_m} f(x,y,z)d\mathbf{r} \approx \sum_{(i,j,k)\in J} f(x_i, y_j, z_k)h^3 \tag{61}$$

where the summation is over J, the set of points inside the surface.

III.B   Solution strategies
III.B.1   Solution of the potential driven geometry flow equation

The solution of potential driven geometric flow equation, or the generalized Laplace-Beltrami equation, has been discussed in our earlier work,[18,42] including many discretization schemes. Here, we present a brief description with an emphasis on different details. An important issue is how to determine all of the physical parameters involved in solving Eq. (53). Some parameters in the literature,[118,148] can be adopted for this purpose. However, due to the nonpolar solvation energy expression in our model, not all parameters can be adopted from the literature. In particular, surface tension γ is used as a fitting parameter in our model due to the ambiguity of its specific value in atomic-scale models.[118,148,214] To this end, we write

$$
\begin{aligned}
\frac{\partial S}{\partial t} &= \|\nabla S\| \left[\nabla \cdot \left(\gamma \frac{\nabla S}{\|\nabla S\|} \right) + V \right] \\
&= \|\nabla S\| \gamma \left[\nabla \cdot \left(\frac{\nabla S}{\|\nabla S\|} \right) + V_\gamma \right]
\end{aligned}
\tag{62}
$$

where $V_\gamma = \frac{V}{\gamma}$. In addition to the Lennard Jones parameters $\bar{\epsilon}_i$, σ_s and σ_i, other parameters that are to be determined in the generalized geometry flow equation are $p/\gamma, \rho_s/\gamma, \epsilon_s/\gamma, \epsilon_m/\gamma$.

Since near the solvent-solution interface, $\|\nabla S\|^2$ is much larger than 1,[18] it does not make a significant difference in practice to modify Eq. (62) as

$$
\frac{\partial S}{\partial t'} = \sqrt{1 + \|\nabla S\|^2} \left[\nabla \cdot \left(\frac{\nabla S}{\sqrt{1 + \|\nabla S\|^2}} \right) + V_\gamma \right]
\tag{63}
$$

where $t' = t\gamma$. This modification is necessary to avoid the possible blowup during the surface evolution where $S_x^2 + S_y^2 + S_z^2$ is very small. For the initial value of S, we consider an indicator function

$$
S(x, y, z, 0) = \begin{cases} S_0, & (x, y, z) \in D \\ 0, & \text{otherwise} \end{cases}
\tag{64}
$$

where we define the domain enclosed by the solvent accessible surface to be $D = \bigcup_{i=1}^{N_a} \{ \mathbf{r} : |\mathbf{r} - \mathbf{r_i}| \leq r_i + r_m \}$, where r_m is the probe radius, $\mathbf{r_i} = (x_i, y_i, z_i), i = 1, \cdots, n$ is the atom center, and r_i represents the radius of the ith atom. Here N_a denotes the total number of the atoms in the molecule. To protect the van der Waals surface and make the computation more efficient, we only update the values of $S(x, y, z, t)$ at the points in between van der Waals surface and solvent accessible surface. i.e., $(x, y, z) \in \bigcup_{i=1}^{N_a} \{ \mathbf{r} : |\mathbf{r} - \mathbf{r_i}| < (r_i + r_m)$ and $|\mathbf{r} - \mathbf{r_i}| >= r_i \}$. In practice, the forward Euler method is employed for time integration, while the second order central different scheme is used for the spatial discretization.[15] Note that the numerical algorithms based on the semi-implicit scheme and alternating-direction implicit (ADI) methods have often been designed and applied.[15] The validity of these methods has been carefully examined.[15,42]

III.B.2   Solution of the Poisson-Boltzmann equation

In general, electrostatic energy is much larger than the non-electrostatic part so that the accuracy of electrostatic potential calculation based on the Poisson-Boltzmann (PB) equation plays a critical role in controlling the accuracy of the total solvation free energy. Therefore, numerical methods that are able to deliver highly accurate solution of the PB equation is desirable. In the present Lagrangian model, there exists a sharp solvent-solute interface and it leads to discontinuous dielectric constant definition in the PB equation. When the continuous dielectric profile is applied across the interface, the standard numerical methods, including the centered finite differences scheme, lose their accuracy and convergent order. This problem is aggravated by complex geometric shapes, possible geometric singularity, and singular charges of biomolecules. In the worst-case scenario, the standard numerical methods do not converge at all for complex irregular solvent-solute interfaces.[82,230]

The solution of elliptic equations with discontinuous coefficients and singular sources is a challenging problem in computational mathematics. In order to achieve high-order numerical accuracy, it is indispensable to develop mathematical interface techniques. Peskin pioneered the immersed boundary method (IBM)[111,162] to address this class of problems. Recently, many other elegant methods have been proposed, including the ghost fluid method,[70,125] the upwinding embedded boundary method,[29] finite-volume-based methods,[152] and integral equation methods.[139] A major advance in the field was due to LeVeque and Li,[117] who proposed a remarkable second order sharp interface scheme, the immersed interface method (IIM).[117,123] Chen and Strain discussed a piecewise-polynomial discretization and Krylov-accelerated multigrid for elliptic interface problems.[40] However, these interface techniques have not been implemented for the Poisson-Boltzmann equation in the context of realistic biomolecules.

We have recently proposed a highly accurate algorithm, the matched interface and boundary (MIB) method[231,232,236,238,239] for solving elliptic equations. Many essential ideas of the current MIB method were introduced in earlier interface schemes for solving Maxwell's equation.[236] The MIB is of arbitrarily high-order accuracy in principle, and sixth-order accurate MIB schemes have been constructed.[231,239] We have developed three generations of MIB based PB solvers, MIBPB-I,[237] MIBPB-II,[230] and MIBPB-III[82] (http://www.math.msu.edu/~wei/MIBPB/). The MIBPB-I is the first PB solver that explicitly enforces the flux continuity conditions at the dielectric interface in a biomolecular context; however, it cannot maintain its designed order of accuracy in the presence of molecular surface singularities, such as cusps and self-intersecting surfaces commonly occurred in biomolecular systems.[173] This problem was first addressed in the MIBPB-II by utilizing an advanced MIB technique developed by Yu et al.;[231] however, the MIBPB-II still loses its accuracy when the mesh size is as large as half of the smallest van der Waals radius, because of the interference of the interface and singular charges. To split the singular charge part of the solution,[27,39,240] a Dirichlet to Neumann mapping approach[46] was designed in the MIBPB-III, which is by far the most accurate and stable PB solver. To our knowledge, the MIBPB method is only existing method that is able to offer second order accuracy in solving the Poisson-Boltzmann equation with discontinuous coefficients, singular sources and arbitrarily complex interfaces. The MIBPB is a few orders of magnitude more accurate at a given mesh size and about three times faster at a given accuracy than some traditional PB solvers.[82]

The most important idea in all interface techniques is to take care of interface conditions, which may vary from systems to systems. Complex interface conditions are needed for the Helmholtz equation[235] and Maxwell's equations.[236] For the Poisson-Boltzmann equation, interface conditions are the following

$$[\phi]_\Gamma = \phi^+(\mathbf{r}) - \phi^-(\mathbf{r}) = 0$$
$$[\epsilon\phi]_\Gamma = (\epsilon_s \nabla\phi^+) \cdot \mathbf{N} - (\epsilon_m \nabla\phi^-) \cdot \mathbf{N} = 0. \tag{65}$$

where ϕ^+ and ϕ^- are the electrostatic potential inside and outside the solvent-solute surface, respectively. Different methods may have different strategies in dealing with these conditions. The MIB method has a unique set of procedures in implementing Eq. (65). The interested reader is referred to our earlier work.[231,232,236,238,239]

In this work, we make use of our MIBPB-III scheme. We take dielectric constants $\epsilon_m = 1$ and $\epsilon_s = 80$ in our calculations. We use the Dirichlet far-field boundary condition and the electrostatic potential values at the boundary are practically obtained by the sum of potential contributions from individual atom charges with an exponential decay factor.[82] The MIBPB-III is used to handle discontinuous dielectric constants, complex geometry and charge singularity. Note that although the geometry is complex, there is no geometric singularities, such as cusps and intersecting surfaces, in the biomolecular surfaces generated by the present approach. The extraction of surface information is carried out by the marching cubes algorithm embedded in our codes.

III.B.3 Dynamic coupling of the Poisson-Boltzmann and geometry flow equations

As described earlier, optimized electrostatic potential ϕ is obtained by solving the Poisson-Boltzmann equation (39) in which solvent-solute interface Γ is used to determine ϵ and λ values. The interface Γ is generated by the solution of the potential driven geometry flow equation (53) which in turn depends on the electrostatic potential. Therefore, the geometry flow equation and the PB equation need to

be solved simultaneously in the present differential geometry based solvation model. In practice, this coupled nonlinear system can be solved by an iterative procedure: First solving the PB equation with a fixed interface Γ for ϕ; Then obtaining the interface Γ from solving the potential driven geometry flow equation with a fixed potential ϕ. A more detailed algorithm follows:

1. Start with an initial solvent-solute interface, such as a solvent accessible surface.

2. Solve the Poisson-Boltzmann equation (39) for the potential with the initial solvent-solute interface.

3. Obtain new solvent-solute interface by solving the potential driven geometry flow equation (53) with the updated potential.

4. Calculate the solvation free energy with the resulting ϕ and Γ.

5. Go back to Step 2 until it converges.

The initial solvent-solute interface can be set by the solvent accessible surface with a probe radius of 1.4 Å. Another way to define the initial geometry is to use the interface obtained from solving the potential driven geometry flow equation (53) without the potential term V. Both approaches lead to the same result. In this study, we take the latter. The iteration will be stopped if the values of total solvation free energy converge to within a designated small criteria value which is 0.01kcal/mol for small molecules and 0.1kcal/mol for proteins in this paper.

III.C   Evaluation of the solvation free energy

The total free energy functional of solvation does not directly provide the total solvation free energy. In the computation of the total solvation free energy, one needs to count only the difference of the system in solvent and in the vacuum. Note that the nonpolar energy already describes the change in free energy; therefore, only the electrostatic energy in vacuum needs to be removed:

$$\Delta G = G - G_0 \tag{66}$$

where G_0 is the polar free energy calculated from the homogeneous (vacuum) environment and is independent of nonpolar energy. Therefore, we have

$$\Delta G = G_{\mathrm{np}} + (G_{\mathrm{p}} - G_0). \tag{67}$$

The expressions of G_{np} and G_{p} are given in Section §II.B. Here $(G_{\mathrm{p}} - G_0)$ can be considered as the polar solvation free energy. In all calculations presented here except for salt effect calculations, mobile ions will be set to zero corresponding to a solution without ion term. Thus, the polar expression is

$$G_{\mathrm{p}} = \int_{\Omega_m} \rho_m \phi d\mathbf{r} - \frac{1}{2} \int_{\Omega} \epsilon(r) |\nabla \phi|^2 d\mathbf{r} = \frac{1}{2} \int_{\Omega_m} \rho_m \phi d\mathbf{r}. \tag{68}$$

Discretizing the integral yields

$$G_{\mathrm{p}} = \frac{1}{2} \sum_{i=1}^{N_m} Q(\mathbf{r}_i) \phi(\mathbf{r}_i), \tag{69}$$

where $Q(\mathbf{r}_i)$ is the ith partial charges at position $\mathbf{r}_i$ inside the biomolecule, N_m is the total number of partial charges. Now the electrostatic solvation free energy can be given by:

$$\Delta G_{\mathrm{p}} = G_{\mathrm{p}} - G_0 = \frac{1}{2} \sum_{i=1}^{N_m} Q(\mathbf{r}_i)(\phi(\mathbf{r}_i) - \phi_0(\mathbf{r}_i)) \tag{70}$$

where ϕ and ϕ_0 are electrostatic potentials in the presence of the solvent and in vacuum, respectively. Here, ϕ is computed from the Poisson equation using the optimized solute-solvent interface

$$-\nabla \cdot (\epsilon(\mathbf{r}) \nabla \phi(\mathbf{r})) = \lambda_m \rho_m \tag{71}$$

23

where $\epsilon(\mathbf{r})$ and ρ_m are the same as those in Eq. (39). The homogeneous solution ϕ_0 is computed with $\epsilon(\mathbf{r}) = \epsilon_m$ in the whole domain. Equation (71) is subject to the far-field boundary condition in principle and the Dirichlet boundary condition in practice.[82] The nonpolar part, G_{np}, is computed exactly by using Eq. (11). The effect of salt concentration is discussed in Section V.B.

IV Validation

This section is devoted to the validation of the proposed differential geometry based solvation model and a number of computational algorithms used in the present work. The overall accuracy of solvation free energy calculation depends on the reliability and accuracy of the solution of the geometry flow equation and the PB solver, surface and volume integrations, and the interface extraction process. The explicit Euler algorithm guarantees the reliability and convergence of the solution of the geometry flow equation. The finite central different scheme is of second order convergence in space and first-order in time although it is computationally expensive.[15] The MIBPB-III has been verified to be of second-order in convergence even with molecular surface singularities of proteins.[82] Therefore, it will be second order accurate for the present application. In fact, the biomolecular surfaces generated with geometric flows are free of geometric singularities, which is computationally easier.

We first examine the impact of the interaction potentials to the surface morphology, and surface electrostatic potentials. A few small molecular systems and 23 protein molecules are used in this examination. We then check the behavior of the surface area under different potential interactions. In particular, we verify whether the proposed minimal molecular surface (MMS)[18] provides the extreme surface area for various molecules and proteins. Finally, we investigate the convergence of the proposed iterative procedure for solving the coupled Poisson-Boltzmann and geometric flow equations.

IV.A Validation of interface extraction

The numerical algorithm for surface integrations has second-order convergence.[83,189] However, the MIBPB-III here has been modified for our purpose to admit the present optimized molecular surface (OMS) as the solvent-solute interface definition. This implies that the reliability of the present MIBPB-III solver depends on the interface extracted by the marching cube algorithm. Moreover, the performance of our surface integration and volume integration algorithms is also determined by the resulting interface instead of some pre-determined interface such as the molecular surface.[170] Therefore, it is worthwhile to validate the interface extraction procedure and algorithm in terms of surface area (Å^2), surface enclosed volume (Å^3) and electrostatic solvation free energy (kcal/mol). In general, there is no analytical result for electrostatic energy except for the one-atom system due to Kirkwood.[108] For the one-atom system without interaction potential, the resulting solvent-solute interface from the geometry flow evolution is a sphere with the same radius as the initial one, for which the PBE admits analytical solution. The surface area and volume can be calculated analytically. Therefore, we consider a dielectric sphere of radii 2Å with a unit charge at the center. We set $\frac{p}{\gamma} = 0.5$, $S_0 = 1000$ and $L = 500$. Table 1 lists the numerical results under different grid resolutions h, which are compared with the exact solution. The convergence in space is observed and satisfactory result is attained.

Table 1: Comparison of surface areas (Å^2), volumes (Å^3) and energies (kcal/mol) for two small systems.

h	One Atom			Two Atom		
	Area	Volume	Energy	Area	Volume	Energy
0.5	48.86	34.00	-84.92	95.24	71.00	-238.03
0.25	49.04	33.56	-82.92	99.28	72.73	-233.66
0.125	50.09	33.52	-82.08	100.5	73.20	-232.37
Referenced Value	50.265	33.510	-81.98	100.34	71.18	-233.67

Another test is done with a diatom system. It has been illustrated previously that molecular surface of a diatom system can be reproduced by our PDE based approach at an appropriate constant potential value.[15] In particular, when the van der Waals (VDW) radii of two atoms are 2Å, the generated surface with $\frac{p}{\gamma} = -0.222$ will be almost identical visually to the molecular surface with probe radius $r_m = 1.4$Å.

In this setting, the corresponding solvation free energy, surface area and volume calculated by our numerical procedure are compared with those based on molecular surface. To calculate the electrostatic solvation energy, a unit charge is set at the centers of two atoms (-2.3,0,0) and (2.3,0,0). The numerical results are summarized in Table 1. For a comparison, the reference molecular surface area and volume of this diatom system are obtained by using the MSMS program[173] with probe radius 1.4 Å and density 100. The electrostatic solvation energy (-233.67 kcal/mol) based on molecular surface is calculated by the original MIBPB-III.[82] A good agreement is also observed from this test.

IV.B   Effect of interaction potentials

In this section, we illustrate the impact of potentials to the generation of solvent-solute interface, consequently to the solvation analysis. Since the effect of the pressure term has already been shown in our previous study, we focus our attention on the study of potential effects which include short-ranged repulsive interaction, long-ranged attractive dispersion interaction and electrostatic potential effect. Here we consider the following 12-6 Lennard-Jones pair potential to model V_i^{LJ},

$$V_i^{\mathrm{LJ}}(\mathbf{r}) = \bar{\epsilon}_i \left[\left(\frac{\sigma_i + \sigma_s}{\|\mathbf{r} - \mathbf{r}_i\|} \right)^{12} - 2 \left(\frac{\sigma_i + \sigma_s}{\|\mathbf{r} - \mathbf{r}_i\|} \right)^6 \right] \tag{72}$$

where $\bar{\epsilon}_i$ is the well-depth parameter, σ_i and σ_s are the radii of solute and solvent, respectively. Here, $\mathbf{r}$ and $\mathbf{r}_i$ are used to represent positions. The L-J potential can be divided into the attractive V^{att} and the repulsive V^{rep} in different ways. It can be a "6-12" decomposition as

$$V_i^{\mathrm{att,LJ}}(\mathbf{r}) = -2\bar{\epsilon}_i \left(\frac{\sigma_i + \sigma_s}{\|\mathbf{r} - \mathbf{r}_i\|} \right)^6 \tag{73}$$

$$V_i^{\mathrm{rep,LJ}}(\mathbf{r}) = \bar{\epsilon}_i \left(\frac{\sigma_i + \sigma_s}{\|\mathbf{r} - \mathbf{r}_i\|} \right)^{12}.$$

It can also be a Weeks-Chandler-Andersen (WCA) decomposition based on the original WCA theory.[219]

$$V_i^{\mathrm{att,WCA}}(\mathbf{r}) = \begin{cases} -\bar{\epsilon}_i(\mathbf{r}) & 0 < \|\mathbf{r} - \mathbf{r}_i\| < \sigma_i + \sigma_s \\ V_i^{\mathrm{LJ}}(\mathbf{r}) & \|\mathbf{r} - \mathbf{r}_i\| \geq \sigma_i + \sigma_s, \end{cases} \tag{74}$$

$$V_i^{\mathrm{rep,WCA}}(\mathbf{r}) = \begin{cases} V_i^{\mathrm{LJ}}(\mathbf{r}) + \bar{\epsilon}_i(\mathbf{r}) & 0 < \|\mathbf{r} - \mathbf{r}_i\| < \sigma_i + \sigma_s \\ 0 & \|\mathbf{r} - \mathbf{r}_i\| \geq \sigma_i + \sigma_s. \end{cases} \tag{75}$$

For the purpose of demonstration, all the surface profiles here are constructed by using 6-12 decomposition and based on the geometry flow Eq. (63) in absence of the pressure term and the ionic effect

$$\frac{\partial S}{\partial t} = \sqrt{1 + \|\nabla S\|^2} \left[\nabla \cdot \left(\frac{\nabla S}{\sqrt{1 + \|\nabla S\|^2}} \right) + \frac{\rho_s}{\gamma} V^{\mathrm{LJ}} - \left(\frac{1}{2} \frac{\epsilon_s}{\gamma} |\nabla \phi|^2 - \frac{1}{2} \frac{\epsilon_m}{\gamma} |\nabla \phi|^2 \right) \right]. \tag{76}$$

Without any potential term, this geometry flow equation leads to minimal molecular surface (MMS).[18] The effects of those three potentials are demonstrated by a diatom system, a four-atom system and finally a protein molecule which is also used to illustrate the potential impacts on surface electrostatic potential analysis. In the present computation, we have treated the solvent density ρ_s as homogeneous.

IV.B.1   Surfaces of a diatom system

We first consider a diatom system with van der Waals radius 1.87Å and coordinates $(x, y, z) = (-2.2, 0, 0)$ and $(2.2, 0, 0)$. Mesh size $h = 0.04$Å is used. The L-J parameters are set as follows: σ_i is taken from atomic radius and σ_s is chosen to be 0.65Å. Well depth $\bar{\epsilon}_i = 0.035$ kcal/mol and bulk density coefficient $\frac{\rho_s}{\gamma} = 2$. To account for electrostatic potential effect, a unit charge is set on the center of each atom and we choose $\frac{\epsilon_s}{\gamma} = 80 * \epsilon_s$ and $\frac{\epsilon_m}{\gamma} = 80 * \epsilon_m$. We use $\epsilon_m = 1$ and $\epsilon_s = 80$ for dielectric constants in solute and solvent, respectively. Figure 2 illustrates the different potential effects on the surface morphology for the diatom system. We systematically change the potential effects to generate different surfaces. We begin
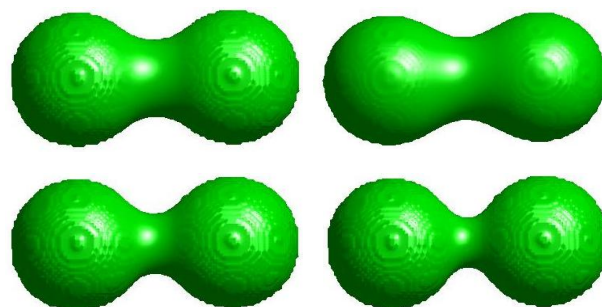
Figure 2: Illustration of surface morphology of a diatom system with radii 1.87Å and coordinates $(x, y, z) = (-2.2, 0, 0)$, and $(2.2, 0, 0)$ under different potentials. Top Left: The MMS (no potential); Top Right: The repulsive potential $(V_i^{\mathrm{rep,LJ}})$; Bottom Left: The attractive potential $(V^{\mathrm{att,LJ}})$; Bottom Right: Electrostatic potential effect.
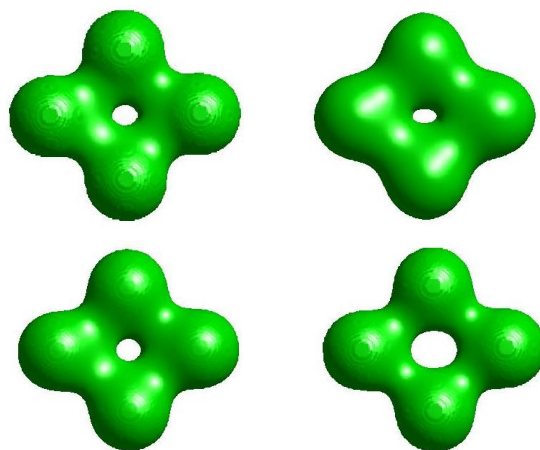

Figure 3: Surfaces of a four-atom system with radii 1.87Å and coordinates $(x, y, z) = (-3.40, 0, 0)$, $(3.40, 0, 0)$, $(0, -2.94, 0)$ and $(0, 2.94, 0)$ under different potentials. Top Left: The MMS (no potential); Top Right: The repulsive potential; Bottom Left: The attractive potential; Bottom Right: Electrostatic potential effect.

with no potential effect, which leads to the minimal molecular surface (Top Left), then add the repulsive part of the L-J potential (Top Right), then add an attractive interaction (Bottom Left) and finally add the electrostatic potential effect in (Bottom Right). It can be seen that the repulsive potential produces a "fat" surface, while an attractive potential or electrostatic potential leads to a "slim" surface. In other words, with a purely repulsive interaction turning on, there is less bulk area between or around two spherical solutes, while more bulk area with attractive potential or electrostatic potential turning on. This result is consistent with experimental observations[215]

IV.B.2 Surfaces of a four-atom system

The effects of potentials on the surface generation are further demonstrated by a four-atom system in Figure 3 with van der Waals radius 1.87 Å and coordinates $(x, y, z) = (-3.40, 0, 0)$, $(3.40, 0, 0)$, $(0, -2.94, 0)$ and $(0, 2.94, 0)$. The needed parameters in Eq. (76) are set as the same as above diatom system except for setting 1/2 charge at the center of each atom. We also systematically change the potential effects by beginning with no potential which leads to the MMS in Fig. 3(Top Left), then add the repulsive part of L-J potential Fig. 3(Top Right), then add the attractive part in Fig. 3(Bottom Left) and finally add

the electrostatic potential effect in Fig. 3(Bottom Right). The impact of potential is similar to that in the diatom system. It is found that the size of hole in the four atoms changes dramatically when varying non-bonding potential. This would imply that the size of pocket or cavity inside a protein can be dramatically changed under different electrostatic potentials and/or solute-solute interaction potentials. Therefore, it may result in a significant difference in physical properties of biological systems, which can dramatically influence the selectivity and gating mechanism of ion channels.

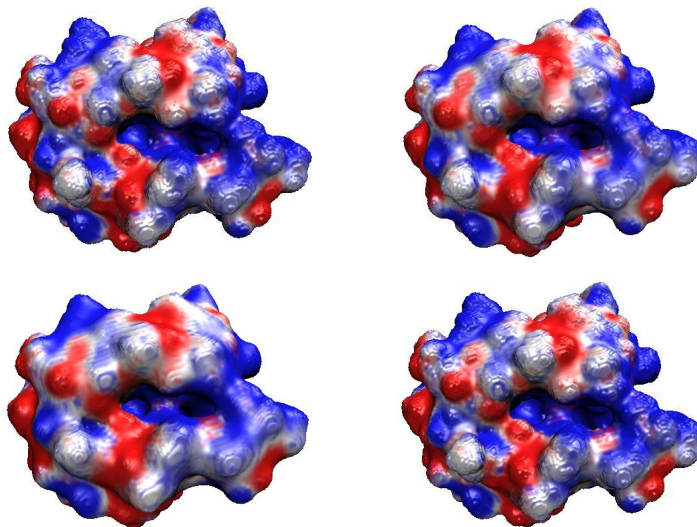### IV.B.3 Surfaces and electrostatic potentials of a protein

Figure 4: Electrostatic surface potentials of protein 451c under different solvent-solute interactions. Top Left: Attractive surface; Top Right: The MMS; Bottom Left: Repulsive surface; Bottom Right: Polar surface.

Table 2: Electrostatic solvation free energies, surface areas and volumes of protein 451c with different solvent-solute interactions.

Surface	Energy (kcal/mol)	Area (Å^2)	Volume (Å^3)
MMS	-724.3	3695.0	12881.9
Repulsive	-635.2	3805.6	13458.3
Attractive	-897.9	3904.9	11635.6
Polar	-838.1	3702.9	12595.7

Having illustrate the effects of various potentials to surface generations for simple artificial systems, we now consider their impacts to surface morphology as well as solvation analysis of proteins. For this purpose, we choose a protein called heme-binding protein, Fe(II) cytochrome C551 from the organism Pseudomonas aeruginosa (PDB ID: 451c). For the structure, extra water molecules that are attached to proteins are excluded and hydrogen atoms are added to obtain a full all-atom model. Partial charges at atomic sites and atomic van der Waals radii in angstroms are taken from the CHARMM22 force field.[134] To show the potential effects, each time we keep one and only one potential term in Eq. (76) to produce a new surface which is used in our PB solver to calculate the electrostatic potential. Starting with the MMS, the surface is called a repulsive surface when only a repulsive potential term is added, an attractive surface when only an attractive interaction is added and a polar surface if only the electrostatic potential effect is allowed. The needed parameters for potential expressions are set in the same way as in the 17 compounds which is described in Section V.A.1. Surface electrostatic potentials are plotted on the corresponding surfaces in Fig. 4. Meanwhile, electrostatic solvation free energies, surface areas and volumes are calculated and listed in Table 2. Potential effects similar to the surface generations of the

diatom and four-atom systems are observed. Moreover, it is interesting to note that the minimal molecular surface (MMS) has the smallest surface area among them so that it indeed minimizes the surface free energy. This is consistent with the mathematical proof that the mean curvature flow equation leads to the minimal surface area. Yet, the MMS does not possess the minimal volume. Instead, the attractive solvent-solute interaction leads to the minimal volume. The repulsive solvent-solute interaction gives rise to the largest volume. These results might appear to be counterintuitive. However, one has to keep in mind that proteins are partially charged molecules. The electrostatic free energy plays a dominant role in the solvent-solute interactions. There is an obvious correlation between the solute volume and the electrostatic free energy: The larger the solute volume is, the smaller the electrostatic free energy is in absolute value. Therefore, the repulsive potential interaction leads to the smallest electrostatic solvation free energy in absolute value, which is an indication of the hydrophobic nature of the repulsive potential interaction. As expected, the attractive solvent-solute interaction leads to the largest electrostatic solvation free energy, reflecting the hydrophilic nature of the attractive solvent-solute interaction. It is believed that the results in Table 2 are very helpful to the understanding of the sophistication of solvation.

IV.C   Isosurface function value and minimal surfaces

Table 3: Surface areas for different surface definitions

| PDB-ID | No.of atoms | Area (Å^2) | |
		OMS	MMS
1ajj	519	2201.4	2046.7
1bbl	576	2657.6	2434.1
1bor	832	2946.9	2683.9
1bpi	898	3274.9	3017.4
1cbn	648	2401.4	2212.7
1fca	729	2728.7	2474.1
1frd	1478	4467.2	3994.2
1fxd	824	3037.3	2762.5
1hpt	858	3368.3	3013.8
1mbg	903	3163.2	2831.3
1neq	1187	4829.0	4295.5
1ptq	795	2959.4	2685.8
1r69	997	3124.8	2806.3
1sh1	702	2808.4	2515.4
1svr	1435	4796.4	4247.9
1uxc	809	2916.1	2630.6
1vii	596	2571.2	2269.3
2erl	573	2380.4	2162.9
2pde	667	2782.0	2527.9
451c	1216	4184.7	3688.5
1a2s	1272	4507.5	3968.7
1a63	2065	7184.8	6369.7
1a7m	2809	7939.4	6918.9

The minimal molecular surface (MMS) proposed in our earlier work[18] was based entirely on the differential geometry theory of surfaces. Although the minimal surface theory is mathematical rigorous, the resulting surface might not be exactly the one with the minimal surface area, when the evolution of the Laplace-Beltrami operator is carried out in the Eulerian representation. This problem is due to the surface extraction process. There are infinitely many ways to select an isosurface value. Our tests indicate that the MMS can be obtained if we choose $L = \frac{S_0}{2}$. Therefore, we set the isosurface function value to 500 in the present solvation free energy calculations rather than a value very close to 1000 which was

used in our earlier paper.[18] The results in Table 2 were obtained in this manner. In this subsection, we further illustrate that the MMS indeed gives rise to the smallest surface area for a set of 23 proteins. Moreover, we also study the impact of the pressure to the surface area for a couple of given protein.

We consider a set of 23 proteins in the present study. The detail of preparation and treatment of protein data is described in Section §V.A.2. Two types of surfaces are generated in the present work. The first type is the MMS constructed by the mean curvature flow.[18] The second type of surfaces is called optimized molecular surface (OMS) generated by using the present differential geometry based solvation model. Results are listed in Table 3. As expected, the surface areas from the MMS model are always smaller that those from the OMS model. Essentially, the minimization of total free energy differ much from the minimization of the surface free energy.

The possession of the minimal surface area in the MMS can be further demonstrated as follows: we consider situations where only the constant pressure (p) is added into the mean curvature flow equation to cause a perturbation of the MMS. For our purpose, two arbitrarily chosen protein systems (PDB-IDs: 1ajj and 451c) from the set of 23 protein are explored. In our simulation, we set $p = -0.4, -0.3, -0.2, -0.1, 0, 0.2, 0.3, 0.4$ and 0.5. The minimal molecular surface is obtained when $p = 0$. Fig. 5 illustrates the difference of surface areas (Å^2) between various resulting surfaces generations under different p values and the MMS for these two protein systems. It is clearly seen that a small perturbation around MMS leads to a larger surface area comparing to that of the MMS. In other words, the MMS indeed has the minimal surface area.
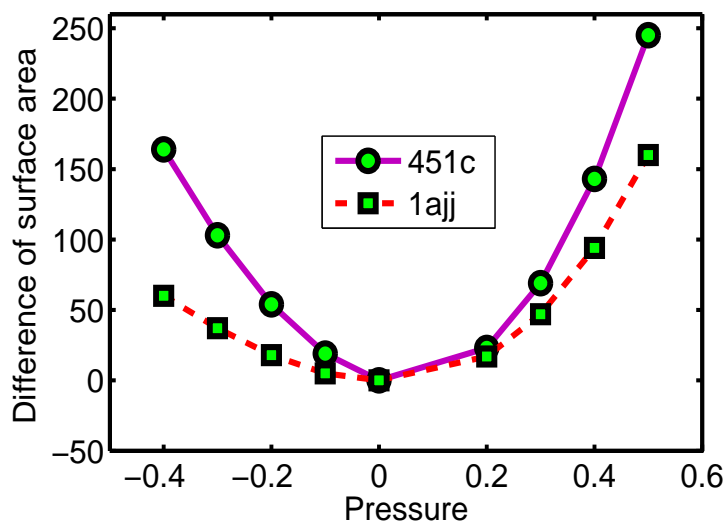

Figure 5: Difference of surface area (Å^2) between MMS and various resulting surface generations under different constant pressure effects.

IV.D   Convergence of surface area, volume and energy

In this section, we illustrate numerically the convergence and decreasing pattern of total solvation free energy during the time integration, which has been shown theoretically in the process of the model derivation. To this end, a small compound named diethyl propanedioate has been chosen from a set of 17 compounds described in Section V.A.1. The time history of the total solvation free energies along with the evolution of solvent-solute boundary is recorded. To illustrate the convergence pattern of the solvation free energy, we compute the total solvation free energies in the intermediate states during the time evolution. The results are shown in Fig. 6. Here T denotes the time span and $N = \frac{T}{\tau}$ represents the number of computational steps in the generalized geometric flow solver. In order to put surface area, enclosed volume and total solvation energy together in one evolution picture, we illustrate J(volume), which is a linear function of volume and shares the same pattern with volume, rather than volume. It is found that the total solvation free energy decreases with respect to the time evolution, which is consistent
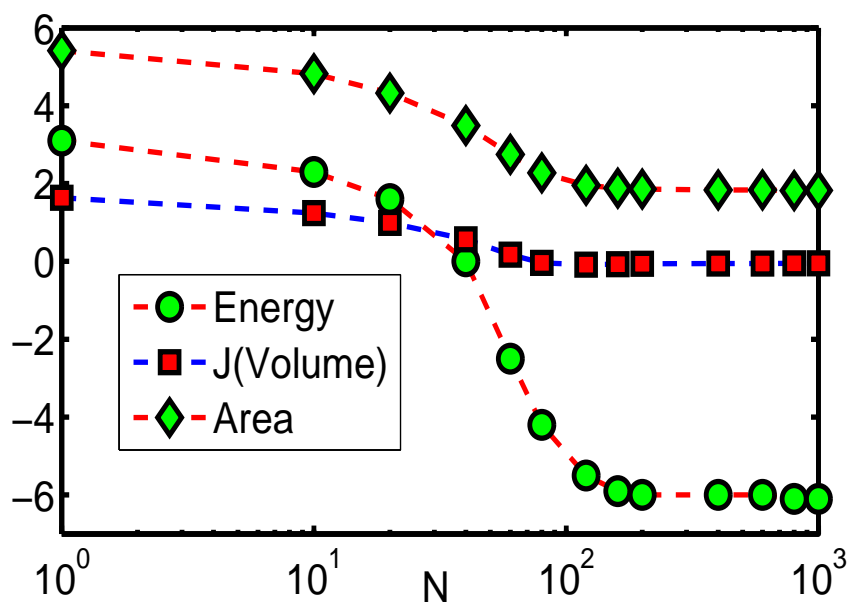
Figure 6: Decreasing of surface area ($\times 10^2$ Å^2),J(volume)=(volume-2) ($\times 10^2$ Å^3) and total solvation free energy (kcal/mol) in diethyl propanedioate

with our theoretical formulation. It is observed that the solution of our model converges to a steady state in terms of volume (Å^3), area (Å^2) and total solvation free energy (kcal/mol).

V Application

In this section, we consider the application of the proposed differential geometry model to the calculations of solvation free energies and salt effects on the protein-protein binding affinity. Previously, we have developed an optimized smooth surface (OSS) model[42] via the Eulerian formulation of the differential geometry based solvation model. It has been demonstrated that OSS model successfully reproduces not only the solvation free energy of small molecules but also the electrostatic solvation free energies of proteins. Although the present optimized molecular surface (OMS) model is derived by using the same framework of free energy functional minimization, the solvent-solute interfaces are entirely different in two models. It is important to verify whether their results are consistent with each other. For a comparison, we choose the same set of 17 compounds used in the previous study.[42] Thus the results from the OSS model are taken directly from the earlier work. In addition, we also choose a subset of 23 proteins from 30 proteins studied in our earlier work.[42] The protein-protein binding affinity is investigated by using two protein systems.

V.A Free energy calculations

V.A.1 Solvation energies of 17 compounds

This test set of 17 small compounds was studied by Nicholls et al.[148] using a number of approaches, including quantum mechanical methods, PB theory etc. It is considered as a challenging test set for computational methods because the existence of polyfunctional or interacting polar groups, which lead to strong solvent-solute interactions. The nonpolar solvent-solute interaction potential in the present model provides a potentially efficient means to deal with strong solvent-solute interactions.

In our calculations, we set the initial amplitude $S_0 = 1000$ and isosurface function value $L = \frac{S_0}{2}$. As in our previous work,[18,42] we set the dielectric constants $\epsilon_m = 1$ and $\epsilon_s = 80$. We use the surface tension γ as a fitting parameter, and its initial value is chosen to be $\gamma = 1/15$ to compute other γ-dependent parameters. We choose $\rho_s/\gamma = 2$ by comparing the bulk density 0.033Å^{-3} and the possible γ value. For microscopic systems, pressure p can be very small and sometimes is neglected in the literature.[43] However, we still take it into account and set $p/\gamma = 0.2$. For L-J parameters, σ_s is chosen to be 0.65Å as

a good fitting solvent radius and σ_i is the solute atomic radii.[214] Given σ_s and σ_i, the value of $\bar{\epsilon}_i$ can be determined by the formula $\bar{\epsilon}_i \left[\left(\frac{\sigma_i + \sigma_s}{\|\mathbf{r} - \mathbf{r}_i\|} \right)^{12} - 2 \left(\frac{\sigma_i + \sigma_s}{\|\mathbf{r} - \mathbf{r}_i\|} \right)^6 \right] = D_i$ which holds if $\mathbf{r}$ is on the vdW surface of the atom. Here the constant D_i should have different values for various types of atoms. For simplicity, we use a uniform constant $D = 1$. We use the grid spacing $h = 0.25$Å and time stepping $\tau = h^2/4.5$ in our applications. Here γ (kcal/(molÅ^2)) serves as a fitting parameter and will have different values for different expressions of nonpolar potential. Details are listed in Table 4. Typically, only attractive solvent-solute interactions contribute to the dispersion effects in the third term of Eq. (11). Here, we have three choices for the dispersion effect: $V^{\mathrm{att,WCA}}$, $V^{\mathrm{att},6/12}$ and V^{LJ}. It turns out that the use of full L-J potential expression can offer the smallest root mean square (RMS) error for the set of 17 compounds. Therefore, it will be chosen from now on for the further study in this paper except specified.

Table 4: RMS error with different nonpolar potentials.

Potential	$V^{\mathrm{att,WCA}}$	$V^{\mathrm{att},6/12}$	V^{LJ}
γ (kcal/(mol Å^2))	0.0077	0.0094	0.0074
RMS (kcal/mol)	1.77	1.83	1.75

Structure and charge information of compounds are adopted from those in Nicholls's paper,[148] which can be obtained from the supplementary information of the paper. In particular, charges are taken from the OpenEye-AM1-BCC v1 parameters.[104] Atomic coordinates and radii are adopted from their new parametrization called ZAP-9 in which certain types of radii are adjusted from Bondi radii to improve the agreement with experimental free energies. Note that with these structures and charges parameters, the root mean square error (RMS) is 1.71 ± 0.05 kcal/mol even using the explicit solvent model. The smallest RMS error of their single-conformer Poisson-Boltzmann approach is 1.87 ± 0.03 kcal/mol.[148] Such a large RMS error indicates the challenge of this test set. The results of the present full L-J potential model are summarized in Table 5. It gives a comparison between the predicted and experimental values of solvation free energies of 17 compounds. The RMS error of the present model is 1.75 kcal/mol. This RMS error is competitive with the explicit solvent approach (1.71 ± 0.05 kcal/mol) under the same charge and structure parameters set.[148] Moreover, it is interesting to note that this the RMS is almost the same as the one obtained from our earlier optimized smooth surface (OSS) model[42] using similar γ value (i.e., 0.0065 kcal/(molÅ^2) vs 0.0074 kcal/(molÅ^2)). This consistency can also be seen through Figure 7 which shows that the results from the OSS and the present OMS are linearly correlated. The correlation coefficient is 0.999. It may reveal at least two facts. First, in the framework of free energy minimization, the calculated results using the Lagrangian representation and the Eulerian representation should be similar to each other. Additionally, a satisfactory nonpolar term and the enforcement of the potential driven geometric flow really play a critical role in the analysis of solvation free energies.

A detailed inspection of Table 5 reveals the fact that large errors are due to benzmides which are from 3.5 to 4.0 kcal/mol. The benzamide problem is likely due to radius adjustment for the carbonyl oxygens and tertiary nitrogens in ZAP 9 under the OpenEye-AM1-BCC v1 charges.[148] In fact, earlier calculations have a similar problem.[42,148] As discussed in our earlier work, one possible solution to this problem is to create a new charge set that is more appropriate for PB approach with the same ZAP radii. This may be realized by introducing quantum mechanical corrections to our model to take care of charge density optimization as well. However, this aspect is out of the scope of the present paper and will be investigated in our future work.

V.A.2   A set of 23 proteins

The set of 17 compounds has already shown the present approach's ability to predict the total solvation free energy of small compounds. Tests on proteins are needed to demonstrate the capacity on the large system of interest. Encouraged by the success in the application to small compounds, we further consider a set of realistic proteins and compare the results with those from previous optimized smooth surface (OSS) model and MIBPB-III[82] with pre-determined molecular surfaces (MSs), which is defined

Table 5: Predicted and experimental total solvation free energies for 17 small compounds.

| Compound	Area (Å^2)	Volume (Å^3)	G_{np}	ΔG_{p}	ΔG	Exptl	Error
					(kcal/mol)		
glycerol triacetate	241.34	234.11	2.33	-12.36	-10.03	-8.84	-1.19
benzyl bromide	150.66	136.36	1.39	-4.87	-3.47	-2.38	-1.09
benzyl chloride	148.14	133.84	1.36	-5.06	-3.70	-1.93	-1.77
m-bis(trifluoromethyl)benzene	266.67	306.86	2.22	-3.30	-1.07	1.07	-2.14
N,N-dimethyl-p-methoxybenzamide	209.31	202.02	1.99	-9.22	-7.22	-11.01	3.79
N,N-4-trimethylbenzamide	200.27	193.25	1.91	-7.84	-5.93	-9.76	3.83
bis-2-chloroethyl ether	155.71	130.90	1.44	-4.16	-2.71	-4.23	1.52
1,1-diacetoxyethane	177.82	160.48	1.67	-8.21	-6.53	-4.97	-1.56
1,1-diethoxyethane	163.66	143.73	1.55	-4.63	-3.08	-3.28	0.20
1,4-dioxane	109.56	143.73	1.01	-5.64	-4.62	-5.05	0.43
diethyl propanedioate	195.06	182.22	1.87	-7.75	-5.88	-6.00	0.12
dimethoxymethane	109.17	88.36	1.02	-4.64	-3.62	-2.93	-0.69
ethylene glycol diacetate	168.19	160.95	1.62	-8.40	-6.78	-6.34	0.44
1,2-diethoxyethane	169.25	141.92	1.57	-4.40	-2.83	-3.54	0.71
diethyl sulfide	133.81	116.84	1.22	-2.40	-1.17	-1.43	0.26
phenyl formate	148.14	134.84	1.37	-7.82	-6.45	-4.08	-2.37
imidazole	89.05	68.59	0.80	-11.56	-10.76	-9.81	-0.95
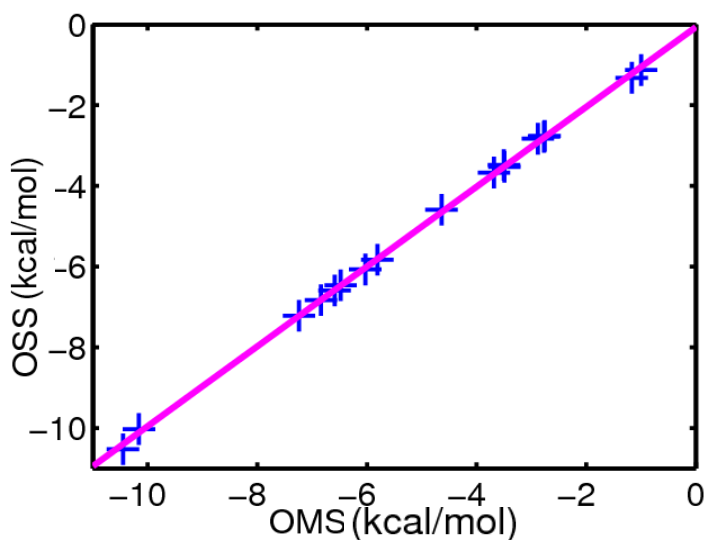
Figure 7: Correlation of solvation free energy between previous optimized smooth surface (OSS) model and the present optimized molecular surface (OMS) model in 17 compound set.

as the inner surface smoothly traced by a probe sphere as it rolls over the atomic sphere.[51,170] Twenty three proteins, a test set used in previous studies,[15,42] are chosen for the present calculations. All structures and partial charges are obtained in the same way as the 451c system which is described before. Table 6 shows the results of the present model, and those of the OSS and the MIBPB-III. Results from the OSS and the MIBPB-III have been proved to be very close to each other and they are competitive to those from quantum mechanic approaches.[42] Like in the set of 17 compounds, results from the OSS and the OMS also show quite consistency. The correlation coefficient between them are 0.999. This can also be observed in the Fig. 8. Therefore, this observation further convinces us that in

the framework of differential geometry based free energy minimization, the OSS and the OMS can be alternative to each other in the aspect of solvation analysis. Since both of them share similar energy functional expressions and take into account the key feature of total energy minimization at equilibrium. If we remove the external potential effects in the surface evolution which are derived from the energy minimization, the present OMS model returns to our previous minimal molecular surface (MMS) model and the calculated results of solvation energies deviate dramatically. Table 3 and Fig. 9 demonstrate the difference of electrostatic solvation free energy between the OSS and MMS models, as well as the difference between the OSS and OMS models. This once again indicates the importance of polar-nonpolar coupling and solute-solvent interaction in implicit solvent modeling and solvation analysis.

Table 6: Comparison of electrostatic solvation free energies of 23 proteins.

PDB-ID	No. of atoms	$\triangle G_\mathrm{p}$(kcal/mol)			
		MIBPB-III	OSS	OMS	MMS
1ajj	519	-1137.2	-1178.5	-1122.3	-921.0
1bbl	576	-986.8	-965.9	-972.0	-792.3
1bor	832	-853.7	-853.7	-836.3	-665.9
1bpi	898	-1301.9	-1281.2	-1295.1	-1060.0
1cbn	648	-303.8	-304.8	-291.0	-181.0
1fca	729	-1200.1	-1200.6	-1184.1	-1040.0
1frd	1478	-2852.2	-2844.8	-2846.7	-2499.5
1fxd	824	-3299.8	-3291.9	-3306.1	-3087.1
1hpt	858	-811.6	-808.2	-815.6	-570.0
1mbg	903	-1346.1	-1328.2	-1346.9	-1148.7
1neq	1187	-1730.1	-1713.9	-1742.9	-1401.6
1ptq	795	-873.1	-866.2	-872.9	-660.2
1r69	997	-1089.5	-1072.7	-1082.7	-824.4
1sh1	702	-753.3	-771.8	-753.9	-532.1
1svr	1435	-1711.2	-1704.6	-1716.7	-1321.3
1uxc	809	-1138.7	-1125.7	-1147.9	-919.3
1vii	596	-901.5	-892.0	-907.0	-724.2
2erl	573	-948.8	-935.8	-944.4	-812.2
2pde	667	-820.9	-843.0	-812.3	-591.3
451c	1216	-1024.6	-1020.6	-1016.8	-718.2
1a2s	1272	-1913.5	-1900.3	-1902.8	-1633.0
1a63	2065	-2373.5	-2380.5	-2382.6	-1851.0
1a7m	2809	-2155.5	-2179.8	-2152.6	-1699.9

V.A.3 Total solvation free energies of proteins

The total solvation free energy of proteins can be computed in the same way as the set of 17 compounds. It is also interesting to compare the calculated total solvation free energies between the present OMS model and other models, particularly SPT.[164,194] To this end, we use the MSMS to generate molecular surfaces,[173] the MIBPB-III[82] to compute electrostatic solvation free energy, and SPT model for the nonpolar solvation free energies. For a comparison, we set the surface tension as $\gamma = 0.0077$ kcal/(molÅ^{-2}) and solvent pressure as $p = 0.00385$ kcal/(molÅ^{-3}) for both approaches. The bulk solvent density of $\rho_0 = 0.033$ Å^{-3} is used for the nonpolar WCA attractive term in the present OMS model. We have picked up the first ten proteins from our earlier 23 protein set to demonstrate the application of the present model. As shown in Table 7, the total free energies computed with two models are in very good agreement. In fact, the proposed differential geometry based OMS model offers lower total free energies of solvation for all proteins examined. However, we should point out that, strictly, the concept of total energy minimization only applies to the same model. Different models might have different minimal values.
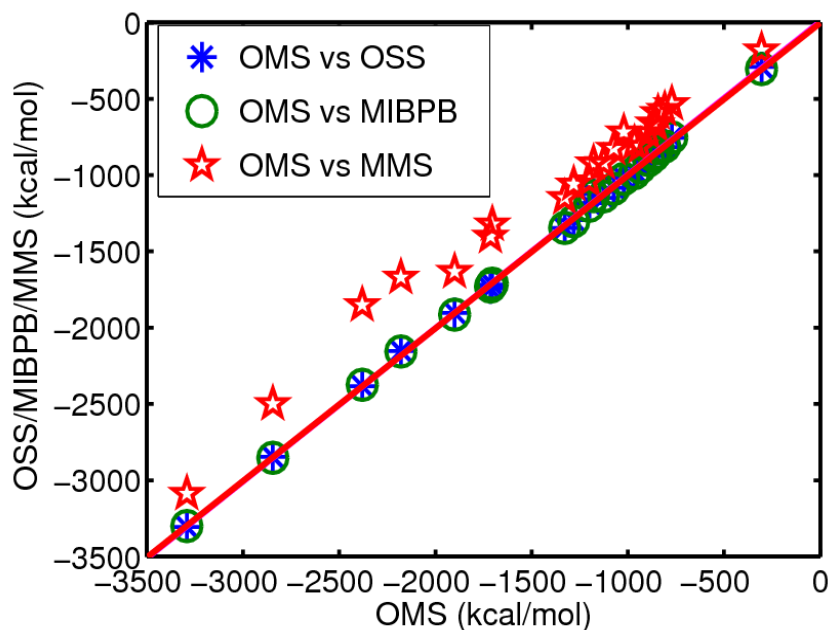
Figure 8: Correlation of electrostatic solvation free energy between the present optimized molecular surface (OMS) model, and previous models, such as the optimized smooth surface (OSS), the MIBPB-III and the MMS for 23 proteins.
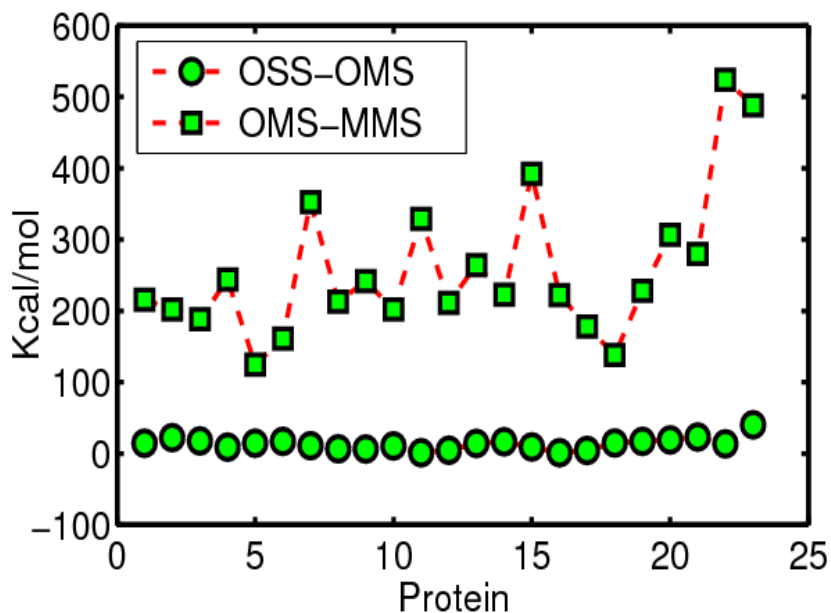

Figure 9: Difference of electrostatic solvation free energy between the OMS model and previous OSS and MMS models.

V.B   Salt effect on protein-protein binding energies

Finally, we consider the application of our differential geometry based solvation model to the calculations of salt effect on the protein-protein binding. This is the first time that our new model is applied to the study of the salt effect. The ion concentration plays an important role in the stability and even reactivity of biomolecules. This application can be further extended to the binding affinity analysis of ligands, peptide, proteins, nucleic acids, and membrane proteins. To this end, the potential terms caused by

34

Table 7: Comparison of total solvation free energies (kcal/mol) for 10 proteins

PDB-ID	1ajj	1bbl	1bor	1bpi	1cbn	1fca	1frd	1fxd	1hpt	1mbg
OMS	-1109.4	-960.0	-824.4	-1272.1	-280.7	-1170.8	-2796.5	-3277.8	-788.3	-1319.1
SPT	-1102.6	-946.8	-803.9	-1246.2	-263.7	-1153.4	-2766.6	-3247.4	-757.0	-1292.3

mobile ions need to be restored in our calculation.

The full Poisson-Boltzmann (39) is coupled to the geometric flow Eq. (53) to obtain the solvation free energy for proteins in the salted solvent. The solution procedure for the nonlinear PB equation was described in our work.[36] The coupling of the nonlinear PB equation and potential driven geometric flow equation is discussed in Section III.B.3. For low salt concentration and weak electrostatic potential, the linearized Poisson-Boltzmann equation discussed in Section II.C.2 can be applied.
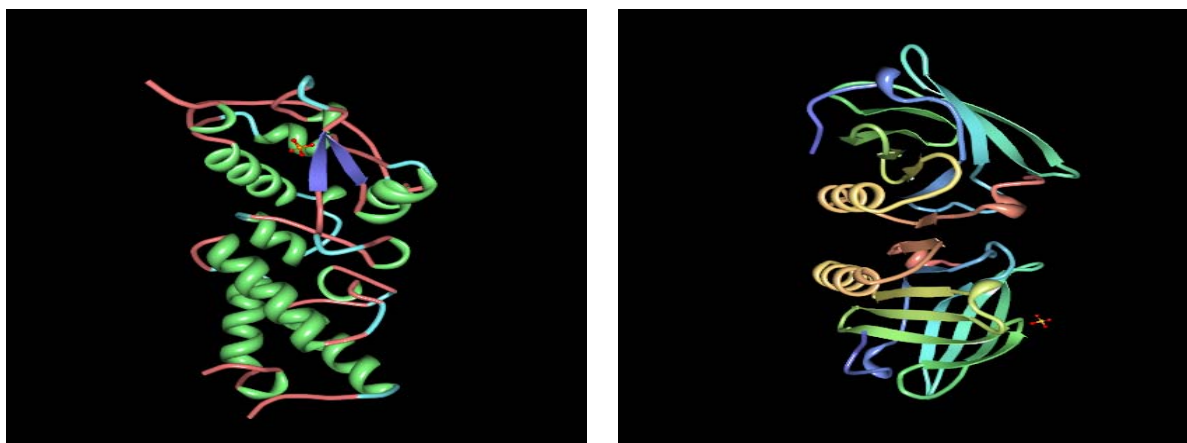

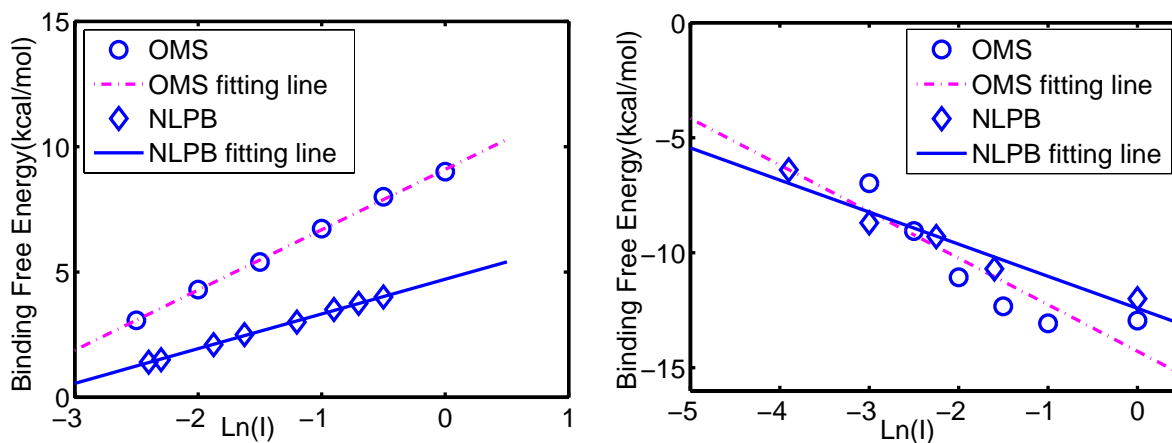Figure 10: Protein-protein complexes. Left: Protein complex 1emv; Right: Protein complex 1beb.

Figure 11: The salt dependence of the binding affinities of two protein complexes. Left: Protein lemv; Right: Protein 1beb. Here OMS data are computed by our optimized molecular surface (OMS) model. NLPB data are taken from Bertonati et al's paper.[23]

For the binding free energy, only the electrostatic component and particularly, its salt dependence are studied. The total binding free energy which includes many other terms that do not depend on the salt concentration, does not need to be calculated. Then the electrostatic component of the binding energy (ΔG_{p}) is found as the difference of the electrostatic free energies of the complex and those of the free

molecules

$$\Delta G_{\mathrm{p}}(I) = G_{\mathrm{p}}^{\mathrm{AB}}(I) - G_{\mathrm{p}}^{\mathrm{A}}(I) - G_{\mathrm{p}}^{\mathrm{B}}(I), \tag{77}$$

where $G_{\mathrm{p}}^{\mathrm{AB}}(I)$, $G_{\mathrm{p}}^{\mathrm{A}}(I)$ and $G_{\mathrm{p}}^{\mathrm{B}}(I)$ are the electrostatic free energies of the complex AB, and the monomers A and B, respectively, at a given ionic strength, I. The salt dependence of the binding free energy $\Delta\Delta G_{\mathrm{p}}(I)$ is thus the difference in the electrostatic components of the binding energies, Eq. (77), attained at some salt concentration I and at zero salt concentration

$$\begin{aligned}
\Delta\Delta G_{\mathrm{p}}(I) &= \Delta G_{\mathrm{p}}(I) - \Delta G_{\mathrm{p}}(I=0) \tag{78}\\
&= \{G_{\mathrm{p}}^{\mathrm{AB}}(I) - G_{\mathrm{p}}^{\mathrm{AB}}(I=0)\}\\
&\quad -\{G_{\mathrm{p}}^{\mathrm{A}}(I) - G_{\mathrm{p}}^{\mathrm{A}}(I=0)\}\\
&\quad -\{G_{\mathrm{p}}^{\mathrm{B}}(I) - G_{\mathrm{p}}^{\mathrm{B}}(I=0)\},
\end{aligned}$$

where each energy term at different ionic strengths can be calculated via Eq. (70). In general, the nonlinear PB equation should be used for the evaluation of salt effects on protein-protein binding. However, as shown by Bertonati et al.,[23] both the linearized PB (LPB) and the nonlinear PB (NLPB) can be applied to calculate salt effects when ionic strength of the salt is weak and the net charges of the binding complex and individual molecules are relatively small. The results obtained with the LPB were very close to those obtained with the NLPB. This encourages us to use LPB in this section to reduce the computational complexity.

Table 8: Comparison of binding affinities of two proteins complexes from current simulations and those from Bertonati et al's paper.

Complex	PDB code	Complex charge	Surface Area (Å^2)	Charge of the free monomers	Bertonati[23]		OMS
					LPB	NLPB	
E9Dnase-Im9 (10)	1emv	-3	1465	B=+5; A=-8	1.29	1.31	2.40
Lactoglobulin Dimer (57) (A-B)	1beb	+26	1167	A=B=+13	-2.48	-1.53	-2.02

To test the utility of our new model in the calculation of salt effects on protein-protein binding, a hetro-dimeric and a homo-dimeric complex are selected for our study. These cases were considered by Bertonati et al.[23] In the experiment, NaCl is used for the salt with a pH value of 3. As shown in Fig. 10, each protein complex encompasses two separated pieces. The structures and charges of them are attained in the same way as earlier 23 proteins, so are the needed parameters in the potential driven geometric flow equation. The salt dependence of the binding free energy from NLPB simulation by Bertonati et al. as well as our OMS model is shown in Fig. 11, where the binding free energy $\Delta\Delta G_{\mathrm{p}}(I)$ is plotted as a function of the logarithm of the salt strength I. Additionally, binding affinities are summarized in Table 8, in which the first four columns describe the properties of proteins and the last two columns are the binding affinities extracted from the slope of the lines in Fig. 11. Note that the calculation is performed by assuming that all Arg, Asp, Glu and Lys residues are ionized in both free and bound states. It is seen that our model clearly reproduces the experimental observation, i.e., for the hetero-dimeric complex, the binding free energies increase with the increasing ionic strength; while for the homo-diemric complex, the affinity is negative. Moreover, as shown in the table the quantities of the binding affinity obtained from simulations with the present OMS model are in good agreement with those obtained by LPB and NLPB methods in Bertonati et al's paper in which NaCl is used for salt with a pH value of 3. Note that in the case of Lactoglobulin dimer, the results obtained with all acidic groups neutral are shown.

VI Concluding remarks

This work is a part of our recent effort in the construction of differential geometry based multiscale models for chemical and biomolecular systems.[42,221] The introduction of differential geometry based

multiscale models is a natural extension of our geometric partial differential equation (PDE) based image analysis[195,220,222] and biomolecular surface generation.[15–18,223] Our previous models make use of a characteristic function so that the description domain is divided into discrete and continuum ones in the Eulerian representation. A smooth domain boundary arises from our previous multiscale models. The objective of the present work is to explore an alternative formulation, the Lagrangian formulation of differential geometry based multiscale solvation models. The Lagrangian representation of biomolecular surfaces is suitable for visualization, surface electrostatic potential map and visual perception of biomolecules. It is can be directly employed in the implicit solvent models and existing software packages. Finally, the Lagrangian representation has an advantage that it avoids artificially enlarging van der Waals radii as often required by smooth surface models.[42,214]

In the present approach, the discrete and continuum domains are separated by a sharp solvent-solute interface, which naturally constitutes a smooth and differentiable manifold enclosing the biomolecule of interest. The time evolution of the manifold is governed by the potential driven geometry flow, a mathematical framework introduced in our previous work.[15,220,221] The specific potential driven geometry flow equation used in the present work is derived via the first variation of the total free energy functional of solvation in the Lagrangian representation. Such a derivation differs much from our earlier derivation using the Eulerian representation and geometric measure theory.[42,221] The total free energy functional of solvation encompasses not only the electrostatic energy, or the polar part, but also the nonpolar solvation energy. The latter includes contributions from surface tension and mechanical work of immersing a molecule into the solvent, which is described as a dielectric continuum in the present model, with a Boltzmann distribution for its ion species. Additionally, another nonpolar term is included to address the issue of solvent-solute interaction and possible solvent density variation in response to the solute effect. The minimization of the total free energy functional gives rise to coupled potential driven geometry flow and Poisson-Boltzmann equations. The resulting potential driven geometry flow equation in the Lagrangian representation is embedded in the Eulerian representation to avoid the geometric singularity development in the Lagrangian dynamics during the time evolution. We show the equivalence of the Laplace-Beltrami operator in two representations. Computational techniques for the interconversion between Lagrangian and Eulerian representations are described in detail. Solution strategies are given to the coupled Poisson-Boltzmann and geometric flow equations. All computational methods and algorithms are carefully validated. The proposed solvation model is applied to the solvation free energy calculations of a set of 17 small compounds and a set of 23 proteins. Results are compared with experimental data or other computational ones. Additionally, we have also demonstrated the usefulness of the present method for the protein-protein binding affinity analysis. Two protein complexes are employed for this analysis and results compare well with experimental measurement.

The spirit of the present free energy minimization approach is similar to that of Sharp and Honig,[183] Gilson et al.,[86] Dzubiella et al.[66,67] and our own work;[16–18] however, there are important differences in the formulation of the nonpolar free energy and computational implementation. The present approach is based on the differential geometry theory of surfaces and it minimizes the surface area and thus, surface free energy in the absence of all other effects, which gives rise to our minimal molecular surface (MMS) first introduced in 2006.[16,18] In contrast, the Dzubiella approach does not minimize surface area and surface free energy at the absence of other effects and instead provides an approach that is more closely tied to the minimization of the combination of Gaussian and mean curvatures, i.e., the Canham-Helfrich curvature type of energy functionals.[31,93] For many years, the Canham-Helfrich curvature energy functional has been providing an important phenomenological model for cell membranes.[102,159] In this model, the bending effect or potential interactions are described macroscopically by high-order curvatures. The Canham-Helfrich curvature energy functional is an extension of the Willmore energy functional[225] which minimizes the difference of the square of the mean curvature and the Gauss curvature. Due to the Gauss-Bonnet theorem, the total curvature is a constant for a given surface topology and the total energy functional becomes non-smooth if there is a topological change (surface breaking and merging) during the surface evolution. Another class of high-order geometric flow models were also proposed in our earlier work[15,220] and used for molecular surface generation.[15] However, unlike the

mean curvature operator that clearly minimizes the surface area as well as the surface free energy of macromolecules, the exact physical role of various high-order curvature models in solvation modeling is yet to be carefully analyzed and explored. In implicit solvent models, since an atomistic description has been given to various interactions in the solute, as well as most of solvent-solute interactions, according to the fundamental laws of physics, the role of phenomenological high-order curvatures can easily become redundant and will be unlikely as important as that in the original Canham-Helfrich model for membrane bending.[31,93]

Although there are some similarities in expressions of coupled PB equation and geometry flow equation between our previous optimized surface (OSS) model[42] and the present optimized molecular surface (OMS) model, there are important differences to be spelled out. First of all, the solute-solvent interface definitions in two models are fundamentally different. In the OSS model, the solute and solvent region is described by a continuous characteristic function denoted by $0 \leq S \leq 1$. In contrast, in the present OMS model, solute and solvent regions are strictly separated by a 2D differentiable manifold. The function S in Eq. (53) only serves as a hypersurface function for geometric surface evolution. This difference has a dramatic computational implication. The generalized Poisson-Boltzmann equation with an OSS is much easier to solve than the OMS is. However, a formal comparison of this computational aspect is beyond the scope of the present work. Moreover, in the potential driven geometry flow equation (53), $\nabla\phi^+ \neq \nabla\phi-$ because of the discontinuity of $\nabla\phi$ inside and outside the solute-solvent interface. However, $\nabla\phi^+ = \nabla\phi^-$ in the overlap region of the OSS model due to continuous dielectric definition. Further, dielectric constant $\epsilon(\mathbf{x})$ in the PB equation is defined in a totally different way: $\epsilon(S)$ is a function of S in the OSS model, and there exists a smooth transition region from the low dielectric to the high dielectric. In contrast, $\epsilon(\mathbf{x})$ is piecewise constant in the present model. In other words, here $\epsilon = \epsilon_s$ in solvent and $\epsilon = \epsilon_m$ in solute, respectively. Further, a generalized Poisson-Boltzmann equation was derived in the OSS model. Whereas, we formally end up with the classical Poisson-Boltzmann equation in the present theory, although it is coupled to the potential driven geometric flow equation. Yet, the present OMS brings up a number of mathematical issues, including the singularity formation on the manifold, and Eulerian embedding of Lagrangian dynamics. Finally, there are many computational problems associated with the Lagrangian formulation of our differential geometry based solvation model too. For instant, the current discontinuous definition of ϵ leads to dramatic accuracy reduction in the standard numerical schemes for the elliptic equations with discontinuous coefficients and singular sources.[231,232,236,238,239] To overcome this difficulty, we have incorporated the highly accurate MIB scheme into our PB solver.[82,230,237] In addition, many other computational issues, such as hybrid Lagrangian and Eulerian dynamics, level set methods, isosurface extraction, surface integration, and Dirichlet to Neumann mapping,[82] are relevant in the present Lagrangian representation.

The present formulation allows the solvent density ρ_s to reflect the density variation near the solvent-solute interface. In principle, such a variation be computed by integral equation approaches of solutions.[20,77,210] Many existing integral equation approaches, including (molecular) density functional theory, hyper-netted chain (HNC) and Percus-Yevick (PY) equations can be used in the present framework to better predict the solvent density profile near the biomolecule. However, the detailed incorporation of the integral equation theory in the solvation calculation is beyond the scope of the present work. As in our previous work,[42] a simple homogeneous solvent density is employed in the present work. The implementation of solvent variation will be considered in the future.

Another important extension of the present work is the implementation of the implicit solvation model based molecular dynamics (MD). Currently, Poisson-Boltzmann (PB) based molecular dynamics algorithms have not been commonly used in the practical simulation of macromolecules. Major hurdles to this development include limits in accuracy, stability, speed and reliability. Typically, low accuracy is due to the lack of the enforcement of interface conditions in solving the Poisson-Boltzmann equation. The stability problem originates from the discontinuous dielectric constants across the solvent-solute interface. The relative low speed is due to the cost of the PB solver and sometimes, the surface generation. All of these problems contribute to the reliability limitation. The multiscale models proposed in this paper and in our recent work[221] have given rise to a new promise for the development of PB based molecular

dynamics algorithms. The accuracy and stability problems in the previous PB based MD methods will not appear in our new model because of the free of dielectric interface.[42] Moreover, in all differential geometric based models, the force expressions differ much from those in the classic Poisson-Boltzmann based MD algorithm as analyzed in our earlier work.[221] The remaining problem is the speed — we must solve an additional geometric flow equation. This challenge will be further investigated in our future work.

Literature cited

[1] J. B. Abrams, L. Rosso, and M. E. Tuckerman. Efficient and precise solvation free energies via alchemical adiabatic molecular dynamics. *The Journal of Chemical Physics*, 125(7):074115, 2006.

[2] C. Amovilli and B. Mennucci. Self-consistent-field calculation of Pauli repulsion and dispersion contributions to the solvation free energy in the polarizable continuum model. *Journal of Physical Chemistry B*, 101(6):1051–1057, 1997.

[3] J. Antosiewicz, J. A. McCammon, and M. K. Gilson. The determinants of pK_as in proteins. *Biochemistry*, 35(24):7819–7833, 1996.

[4] H. S. Ashbaugh. Convergence of molecular and macroscopic continuum descriptions of ion hydration. *Journal of Physical Chemistry B*, 104(31):7235–7238, 2000.

[5] C. Azuara, E. Lindahl, P. Koehl, H. Orland, and M. Delarue. PDB_Hydro: incorporating dipolar solvents with variable density in the Poisson-Boltzmann treatment of macromolecule electrostatics. *Nucleic Acids Research*, 34:W38–W42, 2006.

[6] N. A. Baker. Poisson-Boltzmann methods for biomolecular electrostatics. *Methods in Enzymology*, 383:94–118, 2004.

[7] N. A. Baker. Biomolecular applications of Poisson-Boltzmann methods. In K. B. Lipkowitz, R. Larter, and T. R. Cundari, editors, *Reviews in Computational Chemistry*, volume 21. John Wiley and Sons, Hoboken, NJ, 2005.

[8] N. A. Baker. Improving implicit solvent simulations: a Poisson-centric view. *Current Opinion in Structural Biology*, 15(2):137–43, 2005.

[9] N. A. Baker, D. Bashford, and D. A. Case. Implicit solvent electrostatics in biomolecular simulation. In B. Leimkuhler, C. Chipot, R. Elber, A. Laaksonen, A. Mark, T. Schlick, C. Schutte, and R. Skeel, editors, *New Algorithms for Macromolecular Simulation*. Springer, 2006.

[10] N. A. Baker and J. A. McCammon. Electrostatic interactions. In P. Bourne and H. Weissig, editors, *Structural Bioinformatics*, pages 427–440. John Wiley & Sons, Inc., New York, 2003.

[11] N. K. Banavali, W. Im, and B. Roux. Electrostatic free energy calculations using the generalized solvent boundary potential method. *Journal of Chemical Physics*, 117(15):7381–8, 2002.

[12] V. Barone, M. Cossi, and J. Tomasi. A new definition of cavities for the computation of solvation free energies by the polarizable continuum model. *Journal of Chemical Physics*, 107:3210–3221, 1997.

[13] D. Bashford and D. A. Case. Generalized Born models of macromolecular solvation effects. *Annual Review of Physical Chemistry*, 51:129–152, 2000.

[14] D. Bashford and M. Karplus. pK_a's of ionizable groups in proteins: atomic detail from a continuum electrostatic model. *Biochemistry*, 29(44):10219–25, 1990.

[15] P. W. Bates, Z. Chen, Y. H. Sun, G. W. Wei, and S. Zhao. Geometric and potential driving formation and evolution of biomolecular surfaces. *J. Math. Biol.*, 59:193231, 2009.

[16] P. W. Bates, G. W. Wei, and S. Zhao. The minimal molecular surface. *arXiv:q-bio/0610038v1*, [q-bio.BM], 2006.

[17] P. W. Bates, G. W. Wei, and S. Zhao. The minimal molecular surface. *Midwest Quantitative Biology Conference*, Mission Point Resort, Mackinac Island, MI:September 29 – October 1, 2006.

[18] P. W. Bates, G. W. Wei, and S. Zhao. Minimal molecular surfaces and their applications. *Journal of Computational Chemistry*, 29(3):380–91, 2008.

[19] D. Beglov and B. Roux. Solvation of complex molecules in a polar liquid: an integral equation theory. *Journal of Chemical Physics*, 104(21):8678–8689, 1996.

[20] D. Beglov and B. Roux. An integral equation to describe the solvation of polar molecules in liquid water. *Journal of Physical Chemistry B*, 101(39):7821–6, 1997.

[21] M. Berger and B. Gostiaux. *Differential Geometry: Manifolds, Curves, and Surfaces*. Springer-Verlag, 1988.

[22] C. A. S. Bergstrom, M. Strafford, L. Lazorova, A. Avdeef, K. Luthman, and P. Artursson. Absorption classification of oral drugs based on molecular surface properties. *Journal of Medicinal Chemistry*, 46(4):558–570, 2003.

[23] C. Bertonati, B. Honig, and E. Alexov. Poisson-boltzmann calculations of nonspecific salt effects on protein-protein binding free energy. *Biophysical Journal*, 92:1891–1899, 2007.

[24] A. L. Bertozzi and J. B. Greer. Low-curvature image simplifiers: Global regularity of smooth solutions and Laplacian limiting schemes. *Communications on Pure and Applied Mathematics*, 57(6):764–790, 2004.

[25] N. Blomberg, R. R. Gabdoulline, M. Nilges, and R. C. Wade. Classification of protein sequences by homology modeling and quantitative analysis of electrostatic similarity. *Proteins*, 37(3):379–387, 1999.

[26] P. Blomgren and T. Chan. Color TV: total variation methods for restoration of vector-valued images. *Image Processing, IEEE Transactions on*, 7(3):304–309, 1998.

[27] A. H. Boschitsch and M. O. Fenley. Hybrid boundary element and finite difference method for solving the nonlinear Poisson-Boltzmann equation. *Journal of Computational Chemistry*, 25(7):935–955, 2004.

[28] M. Bostrom, F. W. Tavares, D. Bratko, and B. W. Ninham. Specific ion effects in solutions of globular proteins: Comparison between analytical models and simulation. *Journal of Physical Chemistry B*, 109(51):24489–94, 2005.

[29] W. Cai and S. Z. Deng. An upwinding embedded boundary method for maxwell's equations in media with material interfaces: 2d case. *J. Comput. Phys.*, 190:159–183, 2003.

[30] E. Cances, B. Mennucci, and J. Tomasi. A new integral equation formalism for the polarizable continuum model: Theoretical background and applications to isotropic and anisotropic dielectrics. *Journal of Chemical Physics*, 107:3032 – 3041, 1997.

[31] P. B. Canham. The minimum energy of bending as a possible explanation of the biconcave shape of the human red blood cell. *Journal of Theoretical Biology*, 26:61 – 81, 1970.

[32] V. Carstensen, R. Kimmel, and G. Sapiro. Geodesic active contours. *International Journal of Computer Vision*, 22:61–79, 1997.

[33] T. Cecil. A numerical method for computing minimal surfaces in arbitrary dimension. *Journal of Computational Physics*, 206(2):650–660, 2005.

[34] D. S. Cerutti, N. A. Baker, and J. A. McCammon. Solvent reaction field potential inside an uncharged globular protein: A bridge between implicit and explicit solvent models? *The Journal of Chemical Physics*, 127(15):155101+, 2007.

[35] Q. Chang, X. Tai, and L. Xing. A compound algorithm of denoising using second-order and fourth-order partial differential equations. *NUMERICAL MATHEMATICS-THEORY METHODS AND AP-PLICATIONS*, 2:353–376, 2010.

[36] D. Chen, Z. Chen, C. Chen, W. H. Geng, and G. W. Wei. MIBPB: A software package for electrostatic analysis. *J. Comput. Chem.*, in press, 2010.

[37] D. Chen, G. W. Wei, X. Cong, and G. Wang. Computational methods for optical molecular imaging. *Communications in Numerical Methods in Engineering*, in press.

[38] J. Chen and C. L. Brooks, III. Implicit modeling of nonpolar solvation for simulating protein folding and conformational transitions. *Physical Chemistry Chemical Physics*, 10:471–81, 2008.

[39] L. Chen, M. J. Holst, and J. Xu. The finite element approximation of the nonlinear poisson–boltzmann equation. *SIAM Journal on Numerical Analysis*, 45(6):2298–2320, 2007.

[40] T. Chen and J. Strain. Piecewise-polynomial discretization and krylov-accelerated multigrid for elliptic interface problems. *JOURNAL OF COMPUTATIONAL PHYSICS*, 16:7503–7542, 2008.

[41] Y. G. Chen and J. D. Weeks. Local molecular field theory for effective attractions between like charged objects in systems with strong Coulomb interactions. *Proceedings of the National Academy of Sciences of the United States of America*, 103(20):7560–5, 2006.

[42] Z. Chen, N. A. Baker, and G. W. Wei. Differential geometry based solvation models i: Eulerian formulation. *J. Comput. Phys.*, submitted, 2010.

[43] L. T. Cheng, J. Dzubiella, A. J. McCammon, and B. Li. Application of the level-set method to the implicit solvation of nonpolar molecules. *Journal of Chemical Physics*, 127(8), 2007.

[44] Y. Cheng, J. K. Suen, Z. Radi, S. D. Bond, M. J. Holst, and J. A. McCammon. Continuum simulations of acetylcholine diffusion with reaction-determined boundaries in neuromuscular junction models. *Biophysical Chemistry*, 127(3):129–39, 2007.

[45] Y. Cheng, J. K. Suen, D. Zhang, S. D. Bond, Y. Zhang, Y. Song, N. A. Baker, C. L. Bajaj, M. J. Holst, and J. A. McCammon. Finite element analysis of the time-dependent Smoluchowski equation for acetylcholinesterase reaction rate calculations. *Biophysical Journal*, 92(10):3397–406, 2007.

[46] I.-L. Chern, J.-G. Liu, and W.-C. Weng. Accurate evaluation of electrostatics for macromolecules in solution. *Methods and Applications of Analysis*, 10(2):309–28, 2003.

[47] M. Chiba, D. G. Fedorov, and K. Kitaura. Polarizable continuum model with the fragment molecular orbital-based time-dependent density functional theory. *Journal of Computational Chemistry*, 29:2667–2676, 2008.

[48] D. L. Chopp. Computing minimal surfaces via level set curvature flow. *Journal of Computational Physics*, 106(1):77–91, 1993.

[49] I. Chorny, K. A. Dill, and M. P. Jacobson. Surfaces affect ion pairing. *Journal of Physical Chemistry B*, 109(50):24056–60, 2005.

[50] V. B. Chu, Y. Bai, J. Lipfert, D. Herschlag, and S. Doniach. Evaluation of ion binding to DNA duplexes using a size-modified Poisson-Boltzmann theory. *Biophysical Journal*, 93(9):3202–3209, 2007.

[51] M. L. Connolly. Analytical molecular surface calculation. *Journal of Applied Crystallography*, 16(5):548–558, 1983.

[52] R. B. Corey and L. Pauling. Molecular models of amino acids, peptides and proteins. *Rev. Sci. Instr.*, 24:621–627, 1953.

[53] M. Cossi, V. Barone, R. Cammi, and J. Tomasi. Ab initio study of solvated molecules: A new implementation of the polarizable continuum model. *Chemical Physics Letters*, 255:327–335, 1996.

[54] P. B. Crowley and A. Golovin. Cation-pi interactions in protein-protein interfaces. *Proteins: Structure, Function, and Bioinformatics*, 59(2):231–239, 2005.

[55] L. David, R. Luo, and M. K. Gilson. Comparison of generalized Born and Poisson models: Energetics and dynamics of HIV protease. *Journal of Computational Chemistry*, 21(4):295–309, 2000.

[56] M. E. Davis, J. D. Madura, J. Sines, B. A. Luty, S. A. Allison, and J. A. McCammon. Diffusion-controlled enzymatic reactions. *Methods in Enzymology*, 202:473–497, 1991.

[57] M. E. Davis and J. A. McCammon. Electrostatics in biomolecular structure and dynamics. *Chemical Reviews*, 94:509–21, 1990.

[58] F. De Rienzo, R. R. Gabdoulline, M. C. Menziani, P. G. De Benedetti, and R. C. Wade. Electrostatic analysis and Brownian dynamics simulation of the association of plastocyanin and cytochrome F. *Biophysical Journal*, 81(6):3090–3104, 2001.

[59] C. A. Dietrich, C. E. Scheidegger, J. Schreiner, J. a. L. D. Comba, L. P. Nedel, and C. T. Silva. Edge transformations for improving mesh quality of marching cubes. *IEEE Transactions on Visualization and Computer Graphics*, 15(1):150–159, 2009.

[60] B. N. Dominy and C. L. Brooks, III. Development of a generalized Born model parameterization for proteins and nucleic acids. *Journal of Physical Chemistry B*, 103(18):3765–3773, 1999.

[61] F. Dong, B. Olsen, and N. A. Baker. Computational methods for biomolecular electrostatics. *Methods in Cell Biology*, 84:843–70, 2008.

[62] F. Dong, M. Vijaykumar, and H. X. Zhou. Comparison of calculation and experiment implicates significant electrostatic contributions to the binding stability of barnase and barstar. *Biophysical Journal*, 85(1):49–60, 2003.

[63] F. Dong, J. A. Wagoner, and N. A. Baker. Assessing the performance of implicit solvation models at a nucleic acid surface. *Physical Chemistry Chemical Physics*, 10:4889–902, 2008.

[64] F. Dong and H. X. Zhou. Electrostatic contribution to the binding stability of protein-protein complexes. *Proteins*, 65(1):87–102, 2006.

[65] A. I. Dragan, C. M. Read, E. N. Makeyeva, E. I. Milgotina, M. E. Churchill, C. Crane-Robinson, and P. L. Privalov. DNA binding and bending by HMG boxes: Energetic determinants of specificity. *Journal of Molecular Biology*, 343(2):371–393, 2004.

[66] J. Dzubiella, J. M. J. Swanson, and J. A. McCammon. Coupling hydrophobicity, dispersion, and electrostatics in continuum solvent models. *Physical Review Letters*, 96:087802, 2006.

[67] J. Dzubiella, J. M. J. Swanson, and J. A. McCammon. Coupling nonpolar and polar solvation free energies in implicit solvent models. *Journal of Chemical Physics*, 124:084905, 2006.

[68] S. R. Edinger, C. Cortis, P. S. Shenkin, and R. A. Friesner. Solvation free energies of peptides: Comparison of approximate continuum solvation models with accurate solution of the Poisson-Boltzmann equation. *Journal of Physical Chemistry B*, 101(7):1190–1197, 1997.

[69] A. H. Elcock, R. R. Gabdoulline, R. C. Wade, and J. A. McCammon. Computer simulation of protein-protein association kinetics: Acetylcholinesterase-fasciculin. *Journal of Molecular Biology*, 291(1):149–162, 1999.

[70] R. P. Fedkiw, T. Aslam, B. Merriman, and S. Osher. A non-oscillatory Eulerian approach to interfaces in multimaterial flows (the ghost fluid method). *J. Comput. Phys.*, 152:457–492, 1999.

[71] M. V. Fedorov and A. A. Kornyshev. Unravelling the solvent response to neutral and charged solutes. *Molecular Physics*, 105(1):1–16, 2007.

[72] M. Feig and I. Brooks, C. L. Recent advances in the development and application of implicit solvent models in biomolecule simulations. *Curr Opin Struct Biol.*, 14:217 – 224, 2004.

[73] X. Feng and A. Prohl. Analysis of a fully discrete finite element method for the phase field model and approximation of its sharp interface limits. *Mathematics of Computation*, 73:541–567, 2004.

[74] M. Fixman. The Poisson-Boltzmann equation and its application to polyelectrolytes. *Journal of Chemical Physics*, 70(11):4995–5005, 1979.

[75] F. Fogolari, A. Brigo, and H. Molinari. The Poisson-Boltzmann equation for biomolecular electrostatics: a tool for structural biology. *Journal of Molecular Recognition*, 15(6):377–92, 2002.

[76] J. Forsman. A simple correlation-corrected Poisson-Boltzmann theory. *Journal of Physical Chemistry B*, 108(26):9236–45, 2004.

[77] P. H. Fries and G. N. Patey. The solution of the hypernetted-chain approximation for fluids of nonspherical particles. a general method with application to dipolar hard spheres. *Journal of Chemical Physics*, 82:429 – 440, 1985.

[78] R. R. Gabdoulline and R. C. Wade. Brownian dynamics simulation of protein-protein diffusional encounter. *Methods-a Companion to Methods in Enzymology*, 14(3):329–341, 1998.

[79] E. Gallicchio, M. M. Kubo, and R. M. Levy. Enthalpy-entropy and cavity decomposition of alkane hydration free energies: Numerical results and implications for theories of hydrophobic solvation. *Journal of Physical Chemistry B*, 104(26):6271–85, 2000.

[80] E. Gallicchio and R. M. Levy. AGBNP: An analytic implicit solvent model suitable for molecular dynamics simulations and high-resolution modeling. *Journal of Computational Chemistry*, 25(4):479–499, 2004.

[81] E. Gallicchio, L. Y. Zhang, and R. M. Levy. The SGB/NP hydration free energy model based on the surface generalized Born solvent reaction field and novel nonpolar hydration free energy estimators. *Journal of Computational Chemistry*, 23(5):517–29, 2002.

[82] W. Geng, S. Yu, and G. W. Wei. Treatment of charge singularities in implicit solvent models. *Journal of Physical Chemistry*, 127:114106, 2007.

[83] W. H. Geng and G. W. Wei. Interface technique based implicit solvent molcular dynamics. *J. Comput. Phys.*, submitted, 2008.

[84] R. E. Georgescu, E. G. Alexov, and M. R. Gunner. Combining conformational flexibility and continuum electrostatics for calculating pKas in proteins. *Biophysical Journal*, 83(4):1731–1748, 2002.

[85] G. Gilboa, N. Sochen, and Y. Y. Y Zeevi. Image sharpening by flows based on triple well potentials. *Journal of Mathematical Imaging and Vision*, 20:121–131, 2004.

[86] M. K. Gilson, M. E. Davis, B. A. Luty, and J. A. McCammon. Computation of electrostatic forces on solvated molecules using the poisson-boltzmann equation. *Journal of Physical Chemistry*, 97(14):3591–3600, 1993.

[87] J. Gomes and O. D. Faugeras. Using the vector distance functions to evolve manifolds of arbitrary codimension. *Lecture Notes in Computer Science*, 2106:1–13, 2001.

[88] J. A. Grant, B. T. Pickup, and A. Nicholls. A smooth permittivity function for Poisson-Boltzmann solvation methods. *Journal of Computational Chemistry*, 22(6):608–640, 2001.

[89] J. A. Grant, B. T. Pickup, M. T. Sykes, C. A. Kitchen, and A. Nicholls. The Gaussian Generalized Born model: application to small molecules. *Physical Chemistry Chemical Physics*, 9:4913–22, 2007.

[90] J. B. Greer and A. L. Bertozzi. H-1 solutions of a class of fourth order nonlinear equations for image processing. *Discrete and Continuous Dynamical Systems*, 10:349–366, 2004.

[91] J. B. Greer and A. L. Bertozzi. Traveling wave solutions of fourth order pdes for image processingl. *SIAM Journal on Mathematics Analysis*, 36:38–68, 2004.

[92] P. Grochowski and J. Trylska. Continuum molecular electrostatics, salt effects and counterion binding. a review of the Poisson-Boltzmann theory and its modifications. *Biopolymers*, 89(2):93–113, 2007.

[93] W. Helfrich. Elastic properties of lipid bilayers: Theory and possible experiments. *Zeitschrift für Naturforschung Teil C*, 28:693 – 703, 1973.

[94] C. Holm, P. Kekicheff, and R. Podgornik. *Electrostatic effects in soft matter and biophysics; NATO Science Series*. Kluwer Academic Publishers, Boston, 2001.

[95] M. J. Holst. *Multilevel Methods for the Poisson-Boltzmann Equation*. University of Illinois at Urbana-Champaign, Numerical Computing Group, Urbana-Champaign, 1993.

[96] B. Honig and A. Nicholls. Classical electrostatics in biology and chemistry. *Science*, 268(5214):1144–9, 1995.

[97] T. Hori, H. Takahashi, M. Nakano, T. Nitta, and W. Yang. A qm/mm study combined with the theory of energy representation: Solvation free energies for anti/syn acetic acids in aqueous solution. *Chemical Physics Letters*, 419(1-3):240–244, 2006.

[98] D. M. Huang, P. L. Geissler, and D. Chandler. Scaling of hydrophobic solvation free energies. *Journal of Physical Chemistry B*, 105(28):6704–6709, 2001.

[99] B. Husowitz and V. Talanquer. Solvent density inhomogeneities and solvation free energies in supercritical diatomic fluids: A density functional approach. *The Journal of Chemical Physics*, 126(5):054508, 2007.

[100] W. Im, D. Beglov, and B. Roux. Continuum solvation model: electrostatic forces from numerical solutions to the Poisson-Boltzmann equation. *Computer Physics Communications*, 111(1-3):59–75, 1998.

[101] R. Improta, V. Barone, G. Scalmani, and M. J. Frisch. A state-specific polarizable continuum model time dependent density functional theory method for excited state calculations in solution. *Journal of Chemical Physics*, 125(054103), 2006.

[102] M. Iwamoto, F. Liu, and Z. C. Ou-Yang. Shape and stability of two-dimensional lipid domains with dipole-dipole interactions. *J. Chem. Phys.*, 125:224701, 2006.

[103] R. M. Jackson and M. J. Sternberg. A continuum model for protein-protein interactions: Application to the docking problem. *Journal of Molecular Biology*, 250(2):258–275, 1995.

[104] A. Jakalian, B. L. Bush, D. B. Jack, and C. I. Bayly. Fast, efficient generation of high-quality atomic charges. am1-bcc model: I. method. *Journal of Computational Chemistry*, 21(2):132–146, 2000.

[105] B. Jayaram, D. Sprous, and D. L. Beveridge. Solvation free energy of biomacromolecules: Parameters for a modified generalized Born model consistent with the AMBER force field. *Journal of Physical Chemistry B*, 102(47):9571–9576, 1998.

[106] R. Jinnouchi and A. B. Anderson. Electronic structure calculations of liquid-solid interfaces: Combination of density functional theory and modified poisson-boltzmann theory. *PHYSICAL REVIEW B*, 77(245417), 2008.

[107] S. C. L. Kamerlin, M. Haranczyk, and A. Warshel. Progress in ab initio qm/mm free-energy simulations of electrostatic energies in proteins: Accelerated qm/mm studies of pk(a), redox reactions and solvation free energies. *Journal of Phys. Chem. B*, 113:1253–1272, 2009.

[108] J. G. Kirkwood. Theory of solution of molecules containing widely separated charges with special application to zwitterions. *J. Comput. Phys.*, 7:351 – 361, 1934.

[109] P. Koehl. Electrostatics calculations: latest methodological advances. *Current Opinion in Structural Biology*, 16(2):142–51, 2006.

[110] L. A. Kuhn, M. A. Siani, M. E. Pique, C. L. Fisher, E. D. Getzoff, and J. A. Tainer. The interdependence of protein surface topography and bound water molecules revealed by surface accessibility and fractal density measures. *Journal of Molecular Biology*, 228(1):13–22, 1992.

[111] M. C. Lai and C. S. Peskin. An immersed boundary method with formal second-order accuracy and reduced numerical viscosity. *J. Comput. Phys.*, 160:705–719, 2000.

[112] G. Lamm. The Poisson-Boltzmann equation. In K. B. Lipkowitz, R. Larter, and T. R. Cundari, editors, *Reviews in Computational Chemistry*, pages 147–366. John Wiley and Sons, Inc., Hoboken, N.J., 2003.

[113] D. N. Lebard and D. V. Matyushov. Redox entropy of plastocyanin: Developing a microscopic view of mesoscopic polar solvation. *The Journal of Chemical Physics*, 128(15):155106, 2008.

[114] B. Lee and F. M. Richards. The interpretation of protein structures: estimation of static accessibility. *J Mol Biol*, 55(3):379–400, 1971.

[115] M. S. Lee, J. Salsbury, F. R., and M. A. Olson. An efficient hybrid explicit/implicit solvent method for biomolecular simulations. *Journal of Computational Chemistry*, 25(16):1967–78, 2004.

[116] T. S. Lee, D. M. York, and W. Yang. *The Journal of Chemical Physics*, 105(7):2744–2750, 1996.

[117] R. J. LeVeque and Z. L. Li. The immersed interface method for elliptic equations with discontinuous coefficients and singular sources. *SIAM J. Numer. Anal.*, 31:1019–1044, 1994.

[118] R. M. Levy, L. Y. Zhang, E. Gallicchio, and A. K. Felts. On the nonpolar hydration free energy of proteins: surface area and continuum solvent models for the solute-solvent interaction energy. *Journal of the American Chemical Society*, 125(31):9523–9530, 2003.

[119] H. Li, A. D. Robertson, and J. H. Jensen. The determinants of carboxyl pKa values in turkey ovomucoid third domain. *Proteins*, 55(3):689–704, 2004.

[120] H. Li, A. D. Robertson, and J. H. Jensen. Very fast empirical prediction and rationalization of protein pka values. *Proteins*, 61(4):704–21, 2005.

[121] J. Li, C. L. Fisher, J. L. Chen, D. Bashford, and L. Noodleman. Calculation of redox potentials and pKa values of hydrated transition metal cations by a combined density functional and continuum dielectric theory. *Inorganic Chemistry*, 35(16):4694–702, 1996.

[122] Y. Li and F. Santosa. A computational algorithm for minimizing total variation in image restoration. *IEEE Transactions on Image Processing*, 5(6):987–95, 1996.

[123] Z. L. Li and K. Ito. Maximum principle preserving schemes for interface problems with discontinuous coefficients. *SIAM J. Sci. Comput.*, 23:339–361, 2001.

[124] V. J. Licata and N. M. Allewell. Functionally linked hydration changes in escherichia coli aspartate transcarbamylase and its catalytic subunit. *Biochemistry*, 36(33):10161–10167, 1997.

[125] X. D. Liu, R. P. Fedkiw, and M. Kang. A boundary condition capturing method for Poisson's equation on irregular domains. *J. Comput. Phys.*, 160:151–178, 2000.

[126] D. R. Livesay, P. Jambeck, A. Rojnuckarin, and S. Subramaniam. Conservation of electrostatic properties within enzyme families and superfamilies. *Biochemistry*, 42(12):3464–3473, 2003.

[127] J. R. Livingstone, R. S. Spolar, and J. Record, M. T. Contribution to the thermodynamics of protein folding from the reduction in water-accessible nonpolar surface area. *Biochemistry*, 30(17):4237–44, 1991.

[128] W. E. Lorensen and H. E. Cline. Marching cubes: a high resolution 3d surface reconstruction algorithm. *Computer Graphics*, 21:163–169, 1987.

[129] Q. Lu and R. Luo. A Poisson-Boltzmann dynamics method with nonperiodic boundary condition. *Journal of Chemical Physics*, 119(21):11035–11047, 2003.

[130] R. Luo, L. David, and M. K. Gilson. Accelerated Poisson-Boltzmann calculations for static and dynamic systems. *Journal of Computational Chemistry*, 23(13):1244–53, 2002.

[131] B. A. Luty, M. E. Davis, and J. A. McCammon. Solving the finite-difference non-linear Poisson-Boltzmann equation. *Journal of Computational Chemistry*, 13:1114–1118, 1992.

[132] M. Lysaker, A. Lundervold, and X. C. Tai. Noise removal using fourth-order partial differential equation with application to medical magnetic resonance images in space and time. *IEEE Trans. Imag. Proc.*, 12:1579–1590, 2003.

[133] C. M. MacDermaid and G. A. Kaminski. Electrostatic polarization is crucial for reproducing pKa shifts of carboxylic residues in turkey ovomucoid third domain. *Journal of Physical Chemistry B*, 111(30):9036–44, 2007.

[134] J. MacKerell, A. D., D. Bashford, M. Bellot, J. Dunbrack, R. L., J. D. Evanseck, M. J. Field, S. Fischer, J. Gao, H. Guo, S. Ha, D. Joseph-McCarthy, L. Kuchnir, K. Kuczera, F. T. K. Lau, C. Mattos, S. Michnick, T. Ngo, D. T. Nguyen, B. Prodhom, I. Reiher, W. E., B. Roux, M. Schlenkrich, J. C. Smith, R. Stote, J. Straub, M. Watanabe, J. Wiorkiewicz-Kuczera, D. Yin, and M. Karplus. All-atom empirical potential for molecular modeling and dynamics studies of proteins. *Journal of Physical Chemistry B*, 102(18):3586–3616, 1998.

[135] J. D. Madura, J. M. Briggs, R. C. Wade, M. E. Davis, B. A. Luty, A. Ilin, J. Antosiewicz, M. K. Gilson, B. Bagheri, L. R. Scott, and J. A. McCammon. Electrostatics and diffusion of molecules in solution - simulations with the University of Houston Brownian Dynamics program. *Computer Physics Communications*, 91(1-3):57–95, 1995.

[136] A. V. Marenich, C. J. Cramer, and D. G. Truhlar. Perspective on foundations of solvation modeling: The electrostatic contribution to the free energy of solvation. *Journal of Chemical Theory and Computation*, 4(6):877–887, 2008.

[137] I. Massova and P. A. Kollman. Computational alanine scanning to probe protein-protein interactions: A novel approach to evaluate binding free energies. *Journal of the American Chemical Society*, 121(36):8133–43, 1999.

[138] W. M. Matousek, B. Ciani, C. A. Fitch, B. E. Garcia-Moreno, R. A. Kammerer, and A. T. Alexandrescu. Electrostatic contributions to the stability of the GCN4 leucine zipper structure. *Journal of Molecular Biology*, 374(1):206–19, 2007.

[139] A. Mayo. The fast solution of Poisson's and the biharmonic equations on irregular regions. *SIAM J. Numer. Anal.*, 21:285–299, 1984.

[140] K. Mikula and D. Sevcovic. A direct method for solving an anisotropic mean curvature flow of plane curves with an external force. *Mathematical Methods in the Applied Sciences*, 27(13):1545–1565, 2004.

[141] J. L. Miller and P. A. Kollman. Solvation free energies of the nucleic acid bases. *Journal of Physical Chemistry*, 100(20):8587–8594, 1996.

[142] D. L. Mobley, K. A. Dill, and J. D. Chodera. Treating entropy and conformational changes in implicit solvent simulations of small molecules. *Journal of Physical Chemistry B*, 112(3):938–946, 2008.

[143] V. Mohan, M. E. Davis, J. A. McCammon, and B. M. Pettitt. Continuum model calculations of solvation free energies: accurate evaluation of electrostatic contributions. *Journal of Physical Chemistry*, 96(15):6428–31, 1992.

[144] J. Mongan, C. Simmerling, J. A. McCammon, D. A. Case, and A. Onufriev. Generalized Born model with a simple, robust molecular volume correction. *Journal of Chemical Theory and Computation*, 3(1):159–69, 2007.

[145] Y. Mu, Y. Yang, and W. Xu. Hybrid hamiltonian replica exchange molecular dynamics simulation method employing the Poisson–Boltzmann model. *Journal of Chemical Physics*, 127(8), 2007.

[146] D. Mumford and J. Shah. Optimal approximations by piecewise smooth functions and associated variational problems. *Communications on Pure and Applied Mathematics*, 42(5):577–685, 1989.

[147] R. R. Netz and H. Orland. Beyond Poisson-Boltzmann: Fluctuation effects and correlation functions. *European Physical Journal E*, 1(2-3):203–14, 2000.

[148] A. Nicholls, D. L. Mobley, P. J. Guthrie, J. D. Chodera, and V. S. Pande. Predicting small-molecule solvation free energies: An informal blind test for computational chemistry. *Journal of Medicinal Chemistry*, 51(4):769–79, 2008.

[149] J. E. Nielsen, K. V. Andersen, B. Honig, R. W. W. Hooft, G. Klebe, G. Vriend, and R. C. Wade. Improving macromolecular electrostatics calculations. *Protein Engineering*, 12(8):657–662, 1999.

[150] J. E. Nielsen and G. Vriend. Optimizing the hydrogen-bond network in Poisson-Boltzmann equation-based pK(a) calculations. *Proteins*, 43(4):403–412, 2001.

[151] M. Nina, W. Im, and B. Roux. Optimized atomic radii for protein continuum electrostatics solvation forces. *Biophysical Chemistry*, 78(1-2):89–96, 1999.

[152] M. Oevermann and R. Klein. A cartesian grid finite volume method for elliptic equations with variable coefficients and embedded interfaces. *Journal of Computational Physics*, 219:749–769, 2006.

[153] A. Okur, L. Wickstrom, M. Layten, R. Geney, K. Song, V. Hornak, and C. Simmerling. Improved efficiency of replica exchange simulations through use of a hybrid explicit/implicit solvation model. *Journal of Chemical Theory and Computation*, 2(2):420–433, 2006.

[154] A. Onufriev, D. Bashford, and D. A. Case. Modification of the generalized Born model suitable for macromolecules. *Journal of Physical Chemistry B*, 104(15):3712–3720, 2000.

[155] A. Onufriev, D. A. Case, and D. Bashford. Effective Born radii in the generalized Born approximation: the importance of being perfect. *Journal of Computational Chemistry*, 23(14):1297–304, 2002.

[156] S. Osher and R. P. Fedkiw. Level set methods: An overview and some recent results. *Journal of Computational Physics*, 169(2):463–502, 2001.

[157] S. Osher and L. I. Rudin. Feature-oriented image enhancement using shock filters. *SIAM Journal on Numerical Analysis*, 27(4):919–940, 1990.

[158] S. Osher and J. E. Sethian. Fronts Propagating with Curvature-dependent Speed: Algorithms based on the Hamilton-Jacobi Formulation. *Journal of Computational Physics*, 79:12–49, 1988.

[159] Z. C. Ou-Yang and W. Helfrich. Bending energy of vesicle membranes: General expressions for the first, second, and third variation of the shape energy and applications to spheres and cylinders. *Phys. Rev. A*, 39:5280 – 5288, 1989.

[160] C. S. Page and P. A. Bates. Can MM-PBSA calculations predict the specificities of protein kinase inhibitors? *Journal of Computational Chemistry*, 27(16):1990–2007, 2006.

[161] R. Penfold, S. Nordholm, B. Jnsson, and C. E. Woodward. A simple analysis of ion-ion correlation in polyelectrolyte solutions. *Journal of Chemical Physics*, 92(3):1915–1922, 1990.

[162] C. S. Peskin. Numerical analysis of blood flow in the heart. *Journal of Computational Physics*, 25(3):220–52, 1977.

[163] D. Petrey and B. Honig. GRASP2: Visualization, surface properties, and electrostatics of macromolecular structures and sequences. *Methods in Enzymology*, 374:492–509, 2003.

[164] R. A. Pierotti. A scaled particle theory of aqueous and nonaqeous solutions. *Chemical Reviews*, 76(6):717–726, 1976.

[165] J. W. Ponder and D. A. Case. Force fields for protein simulations. *Advances in Protein Chemistry*, 66:27–85, 2003.

[166] N. V. Prabhu, M. Panda, Q. Y. Yang, and K. A. Sharp. Explicit ion, implicit water solvation for molecular dynamics of nucleic acids and highly charged molecules. *J. Comput. Chem.*, 29:1113 1130, 2008.

[167] N. V. Prabhu, P. Zhu, and K. A. Sharp. Implementation and testing of stable, fast implicit solvation in molecular dynamics using the smooth-permittivity finite difference Poisson-Boltzmann method. *Journal of Computational Chemistry*, 25(16):2049–2064, 2004.

[168] F. H. Quina, E. O. Alonso, and J. P. S. Farah. Incorporation of nonionic solutes into aqueous micelles: a linear solvation free energy relationship analysis. *Journal of Physical Chemistry*, 99:11708–14, 1995.

[169] M. R. Reddy, U. C. Singh, and M. D. Erion. Ab initio quantum mechanics-based free energy perturbation method for calculating relative solvation free energies. *Journal of Computational Chemistry*, 28(2):491–4, 2007.

[170] F. M. Richards. Areas, volumes, packing, and protein structure. *Annual Review of Biophysics and Bioengineering*, 6(1):151–176, 1977.

[171] B. Roux and T. Simonson. Implicit solvent models. *Biophysical Chemistry*, 78(1-2):1–20, 1999.

[172] L. I. Rudin, S. Osher, and E. Fatemi. Nonlinear total variation based noise removal algorithms. In *Proceedings of the eleventh annual international conference of the Center for Nonlinear Studies on Experimental mathematics : computational issues in nonlinear science*, pages 259–268, Amsterdam, The Netherlands, The Netherlands, 1992. Elsevier North-Holland, Inc.

[173] M. F. Sanner, A. J. Olson, and J. C. Spehner. Reduced surface: An efficient way to compute molecular surfaces. *Biopolymers*, 38:305–320, 1996.

[174] G. Sapiro and D. L. Ringach. Anisotropic diffusion of multivalued images with applications to color filtering. *Image Processing, IEEE Transactions on*, 5(11):1582–1586, 1996.

[175] A. Sarti, R. Malladi, and J. A. Sethian. Subjective surfaces: A geometric model for boundary completion. *International Journal of Computer Vision*, 46(3):201–221, 2002.

[176] A. Savelyev and G. A. Papoian. Inter-DNA electrostatics from explicit solvent molecular dynamics simulations. *Journal of the American Chemical Society*, 129(19):6060–1, 2007.

[177] C. Sbert and A. F. Solé. 3d curves reconstruction based on deformable models. *Journal of Mathematical Imaging and Vision*, 18(3):211–223, 2003.

[178] M. Schaefer and M. Karplus. A comprehensive analytical treatment of continuum electrostatics. *Journal of Physical Chemistry*, 100(5):1578–1599, 1996.

[179] D. Sept, A. H. Elcock, and J. A. McCammon. Computer simulations of actin polymerization can explain the barbed-pointed end asymmetry. *Journal of Molecular Biology*, 294(5):1181–1189, 1999.

[180] D. Sept and J. A. McCammon. Thermodynamics and kinetics of actin filament nucleation. *Biophysical Journal*, 81(2):667–674, 2001.

[181] J. A. Sethian. Evolution, implementation, and application of level set and fast marching methods for advancing fronts. *Journal of Computational Physics*, 169(2):503–555, 2001.

[182] Y. Y. Sham, I. Muegge, and A. Warshel. The effect of protein relaxation on charge-charge interactions and dielectric constants of proteins. *Biophysical Journal*, 74(4):1744–1753, 1998.

[183] K. A. Sharp and B. Honig. Calculating total electrostatic energies with the nonlinear poisson-bottzmann equatlon. *Journal of Physical Chemistry*, 94:7684–7692, 1990.

[184] K. A. Sharp and B. Honig. Electrostatic interactions in macromolecules - theory and applications. *Annual Review of Biophysics and Biophysical Chemistry*, 19:301–332, 1990.

[185] T. Simonson. Macromolecular electrostatics: continuum models and their growing pains. *Current Opinion in Structural Biology*, 11(2):243–252, 2001.

[186] T. Simonson. Electrostatics and dynamics of proteins. *Reports on Progress in Physics*, 66(5):737–87, 2003.

[187] T. Simonson and A. T. Brunger. Solvation free energies estimated from macroscopic continuum theory: an accuracy assessment. *Journal of Physical Chemistry*, 98(17):4683–4694, 1994.

[188] P. Smereka. Semi-implicit level set methods for curvature and surface diffusion motion. *Journal of Scientific Computing*, 19(1):439–456, 2003.

[189] P. Smereka. The numerical approximation of a delta function with application to level set methods. *Journal of Computational Physics*, 211(1):77–90, 2006.

[190] N. Sochen, R. Kimmel, and R. Malladi. A general framework for low level vision. *Image Processing, IEEE Transactions on*, 7(3):310–318, 1998.

[191] Y. Song, Y. Zhang, C. L. Bajaj, and N. A. Baker. Continuum diffusion reaction rate calculations of wild-type and mutant mouse acetylcholinesterase: Adaptive finite element analysis. *Biophysical Journal*, 87(3):1558–66, 2004.

[192] Y. Song, Y. Zhang, T. Shen, C. L. Bajaj, J. A. McCammon, and N. A. Baker. Finite element solution of the steady-state Smoluchowksi equation for rate constant calculations. *Biophysical Journal*, 86(4):2017–2029, 2004.

[193] R. S. Spolar, J. H. Ha, and J. Record, M. T. Hydrophobic effect in protein folding and other noncovalent processes involving proteins. *Proceedings of the National Academy of Sciences of the United States of America*, 86(21), 1989.

[194] F. H. Stillinger. Structure in aqueous solutions of nonpolar solutes from the standpoint of scaled-particle theory. *J. Solution Chem.*, 2:141 – 158, 1973.

[195] Y. H. Sun, P. R. Wu, G. W. Wei, and G. Wang. Evolution operator based single-step method for image processing. *Int. J. Biomed. Imaging*, 83847:1–27, 2006.

[196] J. M. J. Swanson, R. H. Henchman, and J. A. McCammon. Revisiting free energy calculations: A theoretical connection to MM/PBSA and direct calculation of the association free energy. *Biophysical Journal*, 86(1):67–74, 2004.

[197] J. M. J. Swanson, J. Mongan, and J. A. McCammon. Limitations of atom-centered dielectric functions in implicit solvent models. *Journal of Physical Chemistry B*, 109(31):14769–72, 2005.

[198] Y. Takano and K. N. Houk. Benchmarking the conductor-like polarizable continuum model (cpcm) for aqueous solvation free energies of neutral and ionic organic molecules. *Journal of Chemical Theory and Computation*, 1(1):70–77, 2005.

[199] C. Tan, Y. H. Tan, and R. Luo. Implicit nonpolar solvent models. *Journal of Physical Chemistry B*, 2007.

[200] C. Tan, L. Yang, and R. Luo. How well does Poisson-Boltzmann implicit solvent agree with explicit solvent? A quantitative analysis. *Journal of Physical Chemistry B*, 110(37):18680–18687, 2006.

[201] J. J. Tan, W. Z. Chen, and C. X. Wang. Investigating interactions between HIV-1 gp41 and inhibitors by molecular dynamics simulation and MM-PBSA/GBSA calculations. *Journal of Molecular Structure: THEOCHEM*, 766(2-3):77–82, 2006.

[202] Z. J. Tan and S. J. Chen. Electrostatic correlations and fluctuations for ion binding to a finite length polyelectrolyte. *Journal of Chemical Physics*, 122:044903, 2005.

[203] M. Tanaka and A. Y. Grosberg. Giant charge inversion of a macroion due to multivalent counterions and monovalent coions: Molecular dynamics study. *Journal of Chemical Physics*, 115(1):567–574, 2001.

[204] C. L. Tang, E. Alexov, A. M. Pyle, and B. Honig. Calculation of pKas in RNA: On the structural origins and functional roles of protonated nucleotides. *Journal of Molecular Biology*, 366(5):1475–96, 2007.

[205] G. J. Tawa, I. A. Topol, S. K. Burt, R. A. Caldwell, and A. A. Rashin. Calculation of the aqueous solvation free energy of the proton. *The Journal of Chemical Physics*, 109(12):4852–4863, 1998.

[206] H. Tjong and H. X. Zhou. GBr6NL: A generalized Born method for accurately reproducing solvation energy of the nonlinear Poisson-Boltzmann equation. *Journal of Chemical Physics*, 126:195102, 2007.

[207] J. Tomasi, B. Mennucci, and R. Cammi. Quantum mechanical continuum solvation models. *Chem. Rev.*, 105:2999–3093, 2005.

[208] V. Tsui and D. A. Case. Molecular dynamics simulations of nucleic acids with a generalized Born solvation model. *Journal of the American Chemical Society*, 122(11):2489–2498, 2000.

[209] V. Tsui and D. A. Case. Calculations of the absolute free energies of binding between RNA and metal ions using molecular dynamics simulations and continuum electrostatics. *Journal of Physical Chemistry B*, 105(45):11314–11325, 2001.

[210] D. M. Tully-Smith and H. Reiss. Further development of scaled particle theory of rigid sphere fluids. *Journal of Chemical Physics*, 53(10):4015–25, 1970.

[211] A. Vitalis, N. A. Baker, and J. A. McCammon. ISIM: A program for grand canonical Monte Carlo simulations of the ionic environment of biomolecules. *Molecular Simulation*, 30(1):45–61, 2004.

[212] A. Vitalis and R. V. Pappu. ABSINTH: a new continuum solvation model for simulations of polypeptides in aqueous solutions. *Journal of Computational Chemistry*, accepted.

[213] R. C. Wade, R. R. Gabdoulline, and F. De Rienzo. Protein interaction property similarity analysis. *International Journal of Quantum Chemistry*, 83(3-4):122–127, 2001.

[214] J. A. Wagoner and N. A. Baker. Assessing implicit models for nonpolar mean solvation forces: the importance of dispersion and volume terms. *Proceedings of the National Academy of Sciences of the United States of America*, 103(22):8331–6, 2006.

[215] A. Wallquist and B. J. Berne. Computer-simulation of hydrophobic hydration forces stacked plates at short-range. *Journal of Physical Chemistry*, 99:2893–2899, 1995.

[216] A. Warshel and A. Papazyan. Electrostatic effects in macromolecules: fundamental concepts and practical modeling. *Current Opinion in Structural Biology*, 8(2):211–7, 1998.

[217] A. Warshel, P. K. Sharma, M. Kato, and W. W. Parson. Modeling electrostatic effects in proteins. *Biochimica et Biophysica Acta (BBA) - Proteins & Proteomics*, 1764(11):1647–76, 2006.

[218] J. Warwicker and H. C. Watson. Calculation of the electric potential in the active site cleft due to alpha-helix dipoles. *Journal of Molecular Biology*, 157(4):671–9, 1982.

[219] J. D. Weeks, D. Chandler, and H. C. Andersen. Role of repulsive forces in determining the equilibrium structure of simple liquids. *Journal of Chemical Physics*, 54(12):5237–47, 1971.

[220] G. W. Wei. Generalized Perona-Malik equation for image restoration. *IEEE Signal Processing Letters*, 6(7):165–7, 1999.

[221] G. W. Wei. Differential geometry based multiscale models. *Bulletin of Mathematical Biology*, pages 1 – 61, 2009.

[222] G. W. Wei and Y. Q. Jia. Synchronization-based image edge detection. *Europhysics Letters*, 59(6):814, 2002.

[223] G. W. Wei, Y. H. Sun, Y. C. Zhou, and M. Feig. Molecular multiresolution surfaces. *arXiv:math-ph/0511001v1*, pages 1 – 11, 2005.

[224] P. Weinzinger, S. Hannongbua, and P. Wolschann. Molecular mechanics PBSA ligand binding energy and interaction of efavirenz derivatives with HIV-1 reverse transcriptase. *Journal of Enzyme Inhibition and Medicinal Chemistry*, 20(2):129–134, 2005.

[225] T. J. Willmore. *Riemannian Geometry*. Oxford University Press, USA, 1997.

[226] K. Wolfgang. *Differential Geometry: Curves-Surface-Manifolds*. American Mathematical Society, 2002.

[227] G. Xu, Q. Pan, and C. L. Bajaj. Discrete surface modeling using partial differential equations. *Computer Aided Geometric Design*, 23(2):125–145, 2006.

[228] M. Xu and S. L. Zhou. Existence and uniqueness of weak solutions for a fourth-order nonlinear parabolic equation. *JOURNAL OF MATHEMATICAL ANALYSIS AND APPLICATIONS*, 325:636–654, 2007.

[229] A. S. Yang, M. R. Gunner, R. Sampogna, K. Sharp, and B. Honig. On the calculation of pK(a)s in proteins. *Proteins-Structure Function and Genetics*, 15(3):252–265, 1993.

[230] S. Yu, W. Geng, and G. W. Wei. Treatment of geometric singularities in implicit solvent models. *Journal of Chemical Physics*, 126:244108, 2007.

[231] S. Yu and G. W. Wei. Three-dimensional matched interface and boundary (MIB) method for treating geometric singularities. *Journal of Computational Physics*, 227:602–632, 2007.

[232] S. Yu, Y. Zhou, and G. W. Wei. Matched interface and boundary (MIB) method for elliptic problems with sharp-edged interfaces. *Journal of Computational Physics*, 224(2):729–756, 2007.

[233] D. Zhang, J. Suen, Y. Zhang, Z. Radic, P. Taylor, M. Holst, C. Bajaj, N. A. Baker, and J. A. Mc-Cammon. Tetrameric mouse acetylcholinesterase: Continuum diffusion rate calculations by solving the steady-state Smoluchowski equation using finite element methods. *Biophysical Journal*, 88(3):1659–65, 2005.

[234] Y. Zhang, G. Xu, and C. Bajaj. Quality meshing of implicit solvation models of biomolecular structures. *Computer Aided Geometric Design*, 23(6):510–30, 2006.

[235] S. Zhao. High order matched interface and boundary methods for the helmholtz equation in media with arbitrarily curved interfaces. *J. Comput. Phys.*, 229:3155–3170, 2010.

[236] S. Zhao and G. W. Wei. High-order FDTD methods via derivative matching for maxwell's equations with material interfaces. *Journal of Computational Physics*, 200(1):60–103, 2004.

[237] Y. C. Zhou, M. Feig, and G. W. Wei. Highly accurate biomolecular electrostatics in continuum dielectric environments. *Journal of Computational Chemistry*, 29:87–97, 2008.

[238] Y. C. Zhou and G. W. Wei. On the fictitious-domain and interpolation formulations of the matched interface and boundary (MIB) method. *Journal of Computational Physics*, 219(1):228–246, 2006.

[239] Y. C. Zhou, S. Zhao, M. Feig, and G. W. Wei. High order matched interface and boundary method for elliptic equations with discontinuous coefficients and singular sources. *Journal of Computational Physics*, 213(1):1–30, 2006.

[240] Z. Zhou, P. Payne, M. Vasquez, N. Kuhn, and M. Levitt. Finite-difference solution of the Poisson-Boltzmann equation: complete elimination of self-energy. *Journal of Computational Chemistry*, 17:1344–1351, 1996.

[241] J. Zhu, E. Alexov, and B. Honig. Comparative study of generalized Born models: Born radii and peptide folding. *Journal of Physical Chemistry B*, 109(7):3008–22, 2005.